Journal of Marine Research, 56, 375–415, 1998

Does the Sverdrup critical depth model explain bloom dynamics in estuaries?

by Lisa **V. Lucas**[1], James E. **Cloern**[2], Jeffrey R. **Koseff**[1], Stephen G. **Monismith**[1] and Janet K. **Thompson**[1,2]

ABSTRACT

In this paper we use numerical models of coupled biological-hydrodynamic processes to search for general principles of bloom regulation in estuarine waters. We address three questions: What are the dynamics of stratification in coastal systems as influenced by variable freshwater input and tidal stirring'? How does phytoplankton growth respond to these dynamics? Can the classical Sverdrup Critical Depth Model (SCDM) be used to predict the timing of bloom events in shallow coastal domains such as estuaries?

We present results of simulation experiments which assume that vertical transport and net phytoplankton growth rates arc horizontally homogeneous. In the present approach the temporally and spatially varying turbulent diffusivities for various stratification scenarios are calculated using a hydrodynamic code that includes the Mellor-Yamada 2.5 turbulence closure model. These diffusivities are then used in a time- and depth-dependent adcection-diffusion equation. incorporating sources and sinks, for the phytoplankton biomass.

Our modeling results show that. whereas persistent stratification greatly increases the probability of a bloom. semidiurnal periodic stratification does not increase the likelihood of a phytoplankton bloom over that of a constantly unstratified water column. Thus, for phytoplankton blooms. the physical regime of periodic stratification is closer to complete mixing than to persistent stratification. Furthermore, the details of persistent stratification are important: surface layer depth, thickness of the pycnoclinc. vertical density difference. and tidal current speed all weigh heavily in producing conditions which promote the onset of phytoplankton blooms.

Our model results for shallow tidal systems do not conform to the classical concepts of stratification and blooms in deep pelagic systems. First. earlier studies (Riley. 1942, for example) suggest a monotonic increase in surface layer production as the surface layer shallows. Our model results suggest, however. a nonmonotonic relationship between phytoplankton population growth and surface layer depth. which results from a balance between several "competing" processes. including the interaction of sinking with turbulent mixing and average net growth occursing within the surface layer. Second, we show that the traditional SCDM must be refined for application to energetic shallow systems or for systems in which surface layer mixing is not strong enough to counteract thc sinking loss of phytoplankton. This need for refinement arises because of the leakage of phytoplankton from the surface layer by turbulent diffusion and sinking. processes not considered in the classical SCDM. Our model shows that, even for low sinking rates and small turbulent

1. Environmental Fluid Mechanics Laboratory. Stanford University. Stanford, California. 94305-4020. U.S.A.
2. U.S. Geological Survey, Middlefield Road, Menlo Park. California, 94025. U.S.A.

diffusivities, a significant percentage of the phytoplankton biomass produced in the surface layer can be lost by these processes.

1. Introduction

In some regions of the world's oceans phytoplankton dynamics are dominated by the spring bloom, a period of rapid population growth that often begins after the water column becomes thermally stratified. The spring bloom is a biological response to physical dynamics, and the mechanism is a discrete change in the balance between phytoplankton primary production and losses when a shallow mixing layer is formed above the seasonal thermocline. This mechanism of the spring bloom was formalized by Sverdrup (1953), who conceived the concept of the critical depth, above which total production is balanced exactly by phytoplankton losses (grazing and respiration). Sverdrup's Critical Depth Model (SCDM) predicts that the spring bloom begins when the depth of the surface mixed layer, Z_m, becomes less than this critical depth, Z_{cr} (Platt *et al.,* 1991. explore the model in detail). Although there have been inconsistencies in the definition of Z_{cr} and challenges to the underlying assumptions of the theory (Smetacek and Passow, 1990). predictions from SCDM are consistent with the timing of the spring blooms in the North Atlantic and western North Pacific (Obata *et al.,* 1996). Deviations between SCDM theory and observations in other regions of the ocean, such as the eastern North Pacific, have motivated research to explore additional mechanisms of bloom regulation such as iron limitation (Martin *et al.,* 1991). So, although Sverdrup's Critical Depth Model does not provide a global predictor of bloom dynamics, it has been a useful tool for interpreting phytoplankton population responses to changing physical dynamics in the upper ocean.

Sverdrup's original problem was the seasonal development of phytoplankton biomass in the open ocean as a response to seasonal stratification by heat input. In shallow coastal waters, other mechanisms of physical variability can overwhelm the annual cycle of thermal stratification. For example, in estuaries and shallow shelf waters (regions of freshwater influence, Simpson *et ml.,* 1991), salinity stratification can be a stronger stabilizing force than thermal stratification. However, even the stabilizing influence of freshwater inputs can be offset by the strong turbulent mixing of shallow waters by tidal currents and wind stress. As a result, shallow coastal systems have more complex stratification dynamics than the open ocean, with components of variability associated with seasonal and event-scale fluctuations of river flow as well as the semidiurnal and weekly fluctuations in tidal energy (Simpson *et al.,* 1990). These shallow coastal systems also have more complex population dynamics of phytoplankton, with episodic and high-amplitude fluctuations of biomass superimposed onto seasonal cycles (Cloern, 1996). Although much of this biomass variability is correlated with fluctuations in stratification driven by the seasonal variability of river flow and hourly-daily variability of tidal stirring (Sinclair *et al.,* 1981), we have not yet developed a general theory to define the physical conditions under which phytoplankton blooms can develop in shallow coastal waters. We ask here if the critical depth concept can be used to explain the association between stratification dynamics and bloom dynamics in shallow coastal systems such as estuaries.

This paper is the third in a series to explore the linkages between bloom dynamics and physical dynamics of shallow coastal waters. Our approach is to use an evolving numerical model of coupled biological-hydrodynamic processes to search for general principles of bloom regulation in estuarine waters. In the first paper (Cloern, 1991) we showed how phytoplankton population growth can change in response to daily fluctuations in vertical mixing over the neap-spring cycle. In the second paper (Koseff *et al.,* 1993) we showed the importance of hourly-scale fluctuations in mixing over the semidiurnal tide cycle. and that stratification is a necessary condition for bloom inception in shallow (~10 m deep) waters where algal production is constrained by light availability and where losses can include rapid consumption by benthic invertebrates. In this paper. we extend this theoretical foundation to show how the details of salinity stratification influence the development of blooms. Blooms can arise from many different mechanisms. For example, in a certain class of systems (e.g. Georges Bank. see Franks and Chen, 1996) the presence of fronts is very important for the occurrence of phytoplankton blooms, whereas for other systems, such as Puget Sound (Winter *et al.,* 1975), the York River estuary (Haas *et al.,* 1981), and the lower St. Lawrence estuary (Sinclair. 1978), blooms develop when the local balance between production and consumption processes is changed by the establishment of vertical density stratification. We therefore consider here only the importance of local processes of algal production-consumption-transport that can be included in the framework of a vertical one-dimensional model. In the next phase of our analysis we will consider the additional importance of advective processes by extending the model to include horizontal variability and transports.

The marine domains considered here are very different physical systems from the deep pelagic domain originally considered by Sverdrup. In his exploration of the spring bloom in the Norwegian Sea. Sverdrup followed the weekly development of thermal stratification that forms surface layers tens to hundreds of meters deep. Here, we consider the hourly fluctuations of salinity stratification that forms surface layers shallower than ten meters in thickness. In Sverdrup's pelagic system, the primary mechanisms of phytoplankton loss were conceived to be respiration and zooplankton grazing. Here, we consider shallow pelagic systems strongly connected to the benthos, which is an additional (sometimes dominant) sink for phytoplankton production. Additionally, the portion of the water column which Sverdrup studied was much less turbid than the shallow systems we are considering. Thus, the values of Z_{cr} associated with the system we are studying are generally much smaller than those of Sverdrup. Therefore, our search for principles of bloom regulation in estuaries must consider additional processes as well as physical dynamics operating at different spatial and temporal scales from those originally conceived by Sverdrup. With this framework in mind. we designed model experiments to address the following questions: (1) What are the dynamics of stratification in coastal systems as influenced by variable freshwater inputs and tidal stirring? (2) How does phytoplankton population growth respond to these stratification dynamics? Is there a simple monotonic relation between population growth and the depth of the mixed layer, as suggested by Riley

(1942)? (3) Can the critical depth criterion (blooms occur whenever $Z_m/Z_{ci} < 1$) be used to predict the timing of bloom events in estuaries?

2. The Physical system

a. Stratification in estuaries

It is well known that the stabilizing effect of density stratification has a profound influence on vertical mixing rates and thus on phytoplankton bloom dynamics (Cloern, 1991: Koseff *et al.*, 1993; Cloern, 1996). Hence, in shallow coastal waters where stratification often results from interactions between buoyancy inputs from rivers and turbulent mixing associated with tides. winds. and density-driven flows, the formation of stratification is one means by which variations in physical forcing can influence biology (Officer, 1976). The precise mechanisms of stratification development, as well as the strength of stratification, however, can vary from system to system. For example. in fjords such as Puget Sound or salt wedges such as the Mississippi Kiver, mixing is relatively weak, allowing strong, permanent stratification to develop. In these flows, local salinity and velocity fields can be controlled hydraulically much in the way open channel flows are controlled by weirs (Armi and Farmer, 1986). In partially mixed estuaries, however, mixing is strong and vertical stratification is weak or nonexistent, with horizontal density gradients dominating trends in density variation (Offices, 1976). In their dynamically based classification scheme for estuaries, Jay and Smith (1990a) refer to these as partially stratified estuaries, reflecting the significance of even weak stratification. This partially mixed/stratified estuary best describes the shallow, strongly tidally mixed system considered here.

Simpson *et al.* (1990) have described and analyzed an important stratification mechanism, known as Strain Induced Periodic Stratification (SIPS), for partially mixed/stratified estuaries where a longitudinal salinity gradient exists between the ocean and the freshwater source. Their description is as follows and is sketched in Figure 1. Assume we start with a homogeneous water column at the start of the flooding tide (Fig. 1a). During the flood tide (Fig. 1b), salty water is carried over fresher water by the vertically sheared tidal current, producing unstable stratification and thus inducing vertical mixing. In this case, the vertical shear in the horizontal current is due only to the presence of the bottom boundary layer. However, on the ebb (Fig. 1c), stable stratification develops when the sheared tidal current carries fresher water over salty water. This stratification reduces the vertical mixing of momentum and increases the velocity shear (Monismith and Fong. 1996), further increasing the rate of stratification production (Jay and Musiak, 1996; Nepf and Geyer, 1996).

Depending on the strength of the tidal currents, turbulent mixing can eliminate the stratification before the end of the ebb, or the water column can remain stratified into the next flood tide. This process can be periodic on longer time scales, with the stratification strengthening during neap tides and weakening during spring tides (Simpson *et al.*, 1990:

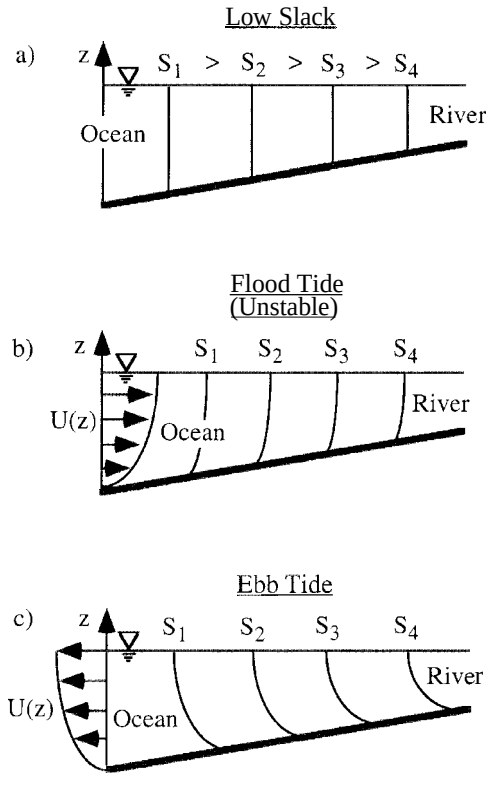

Figure 1. Schematic of SIPS mechanism: (a) assume at low slack, isohalines are vertical (vertically well mixed): (b) on flood. unstable stratification (and imminent mixing) may occur; (c) on ebb, shear strains salinity field, stabilizing water column (after Simpson *et al.*, 1990).

Nunes Vaz and Simpson, 1994). A sample of this process is seen in Figure 2, a plot of Spring 1995 data for South San Francisco Bay (Friebel *et al.*, 1996). In this figure, the salinity difference between sensors located at mid-depth and near-bottom of the 15 m deep water column is plotted as a function of time for a station near the San Mateo Bridge. The predicted daily maximum tidal current speed for a station near the San Mateo Bridge is plotted as well (Cheng and Gartner, 1985). The vertical salinity difference displays a semidiurnal oscillation throughout the record. indicating the presence of tidal straining (SIPS). In addition, during the neap tides (when the daily maximum current speed is relatively low), the stratification does not break down completely on the semidiurnal timescale but, rather, persists for a number of days. Similar observations have been made in other estuaries, notably the York (Sharples *et al.*, 1994), Columbia (Jay and Smith, 1990b), Hudson (Nepf and Geyer, 1996), Spencer Gulf (Nunes Vaz *et al.*, 1989), and the Tamar (Uncles and Stephens, 1990). Evidently, SIPS is a common feature of a large class of estuaries.

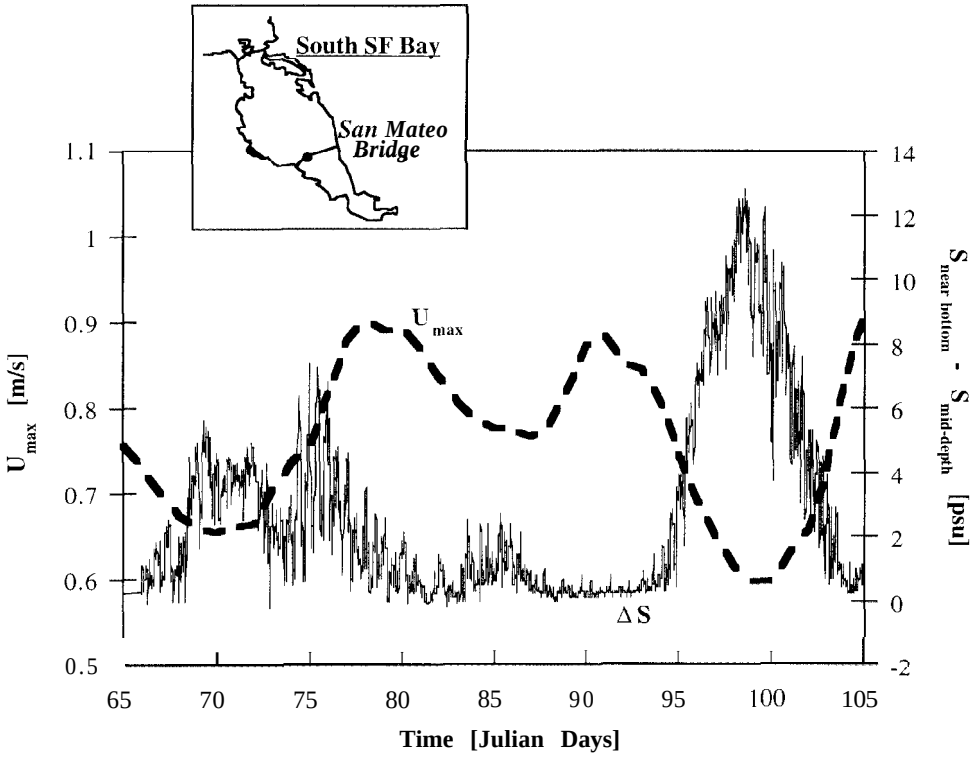

Figure 2. Vertical salinity difference (Friebel *et al.*, 1996) and maximum tidal current speed (Cheng and Gartner, 1985) at San Mateo Bridge, south San Francisco Bay, Spring 1995. Salinity data were measured by *in situ* instruments; the current speeds were calculated by a tidal prediction program which uses harmonic constants derived from field data.

Monismith *et al.* (1996) argued that the SIPS condition only occurs in a one-dimensional channel when

$$Ri_x = \frac{g\dfrac{\partial \rho}{\partial x}H^2}{\rho_o C_D U_{max}^2} \leq O(1) \qquad (1)$$

where Ri, is a stability parameter: g is gravitational acceleration; $\partial\rho/\partial x$ is the longitudinal density gradient [kg/(m^3−m)] (assumed to be constant over the flow depth and in time); H is the depth of the channel: U_{max} is the maximum tidal velocity on the surface; C_D is the bottom drag coefficient; and ρ_o is the reference density. This condition is based upon the assumption of a local one-dimensional balance of salinity and momentum (i.e., replacing the estuary with a fictional one-dimensional channel), and is supported by modeling (using the methods and code described below) and salinity data from northern San Francisco Bay.

When Ri, is greater than about 1, the stratification strengthens each tidal cycle, a

condition referred to as "persistent" or "runaway" stratification. While the fundamental structure assumed by the model may be oversimplified, the general picture inferred by Monismith *et al.* (1996) appears consistent with field measurements. Model runs conducted in the course of the present study (to be reported elsewhere) suggest that the critical condition is also a function of the tidal excursion, behavior that most likely reflects the temporal element of flow evolution. Runaway stratification appears to be attributable to the strong nonlinearity that comes from the longitudinal salinity gradient; it provides the baroclinic pressure gradient that drives a flow which always acts to stratify. as well as providing the "source" term for the stratification itself. As the water column stratifies, the baroclinic flow strengthens (Jay and Musiak, 1996; Monismith *et al.*, 1996), thus intensifying the stratification and further reducing the mixing rates. Since this sheared flow is superimposed on the tides, it ultimately can overcome the destratification that takes place on the floods.

b. Modeling stratified estuarine turbulence

At the simplest level. hydrodynamic processes only affect modeled phytoplankton behavior through the spatial (vertical) and temporal variations in eddy diffusivity (Cloern, 1991). This relationship can either be provided by using assumed eddy diffusivities (as was done by Cloern, 1991, and Koseff *et al.*, 1993) or by modeling which connects forcing (i.e. horizontal pressure gradients and salinity gradients) directly to stratification and velocity shear, and hence to parameterizations of mixing (i.e. turbulent diffusivities). Intermediate steps in which stratification is specified and held fixed while the velocity and turbulence fields evolve are also possible. The full modeling approach can be used to model SIPS or the evolution of runaway stratification; the intermediate approach can be used to model fjords or other systems with persistent stratification, or periods of runaway stratification that occur during neap tides.

The hydrodynamic model we use follows the approach of Hamblin (1989) and Simpson and Sharples (1991): we solve momentum, salt and turbulence balance equations representing turbulent flow in a hypothetical one-dimensional estuary; i.e., the governing momentum and salt conservation equations are simplified to retain only vertical variability in the velocities and salinities. For the momentum balance, this is accomplished by neglecting advective accelerations and by specifying tidal and nontidal barotropic pressure gradients as well as a nontidal baroclinic pressure gradient. The salinity we compute only varies in the vertical; however, since horizontal advection of salt plays a key role in the formation of stratification, we follow Simpson and Sharples (1991) and introduce a source term that represents the effects of horizontal advection. That is, the total salinity at a point is assumed to be of the form:

$$S(x, z, t) = \Gamma x + S'(z, t) \tag{2}$$

where Γ, the mean longitudinal salinity gradient, is a constant. Under these conditions, the

salinity. S', evolves according to a balance between unsteady change. diffusion, and horizontal advection, i.e.:

$$\frac{\partial S'}{\partial t} - \frac{\partial}{\partial z}\left(K_s \frac{\partial S'}{\partial z}\right) = -U\Gamma \tag{3}$$

where $K_s(z, t)$ is the eddy diffusivity for salt, and $U(z, \mathrm{r})$ is the computed horizontal velocity. Note that it is vertical variability in U that gives rise to stratification through the SIPS mechanism outlined above. In order for this approximation to remain valid, we must assume that Γ *does not vary* with x. Variations with time as well as with depth can be included without altering the model structure (Simpson and Sharples. 1991).

The momentum balance is that used by Simpson and Sharples (1991) as implemented by Monismith *et al.* (1996) and summarized here. The barotropic tide is represented by a known time varying surface slope

$$\frac{\partial \zeta}{\partial x} = -\frac{U_{max}}{g}\left(\frac{2\pi}{T}\right)\cos\left(\frac{2\pi}{T}t\right) \tag{4}$$

where ζ is the hypothetical variation in water surface elevation necessary to drive an inviscid tidal flow with a maximum velocity of U,,,,,,(see discussion in Monismith and Fong, 1996) and period T (we use T ~ 12 h, i.e., roughly an M_2 tide). For simplicity, we consider only a single tidal constituent: however, multiple constituents can also be used. The horizontal salinity gradient, Γ, which we specify, provides a baroclinic pressure gradient that is independent of x and increases linearly with depth. To account for the surface slope associated with the baroclinic flow. an extra constant surface pressure gradient equal to a dimensionless constant, y. multiplied by the depth-averaged baroclinic pressure gradient is imposed. 'l'he constant γ determines the tidally averaged flow that results. In our application, we iteratively found γ (typically in the range -0.1 to -0.5) to minimize the net depth-averaged flow over a tidal cycle. Note that the flow depth is not allowed to change through the tide: the barotropic pressure gradients we impose are only expressed in terms of surface slopes for the sake of convenience.

With these assumptions and this structure, the momentum balance is:

$$\frac{\partial U}{\partial t} - \frac{\partial}{\partial z}\left(\epsilon_s \frac{\partial U}{\partial z}\right) = -g\frac{\partial \zeta}{\partial x} - g\beta\Gamma\left(-z + \gamma\frac{H}{2}\right) \tag{5}$$

where ϵ_s is the eddy viscosity, β is the coefficient of saline expansivity (such that $\beta\Gamma \sim (1/\rho_o)(\partial\rho/\partial x)$), and z is the depth measured negative downward from the surface.

The turbulent diffusivities are found using Galperin et *al.*'s (1988) version of the Mellor-Yamada level 2.5 (MY2.5) closure commonly used to model turbulence in geophysical flows (Mellor and Yamada. 1982: Blumberg and Goodrich. 1990). MY2.5 defines eddy mixing coefficients as the products of a turbulence velocity scale (q), a

turbulence lengthscale (l), and stability functions. S_m and S_H, designed to represent the effects of stratification on turbulent mixing:

$$\epsilon_z = S_m q l \tag{6}$$

$$K_z = S_H q l. \tag{7}$$

S_m and S_H are given as functions of the turbulent Froude number

$$Fr_t = \frac{q}{Nl} \tag{8}$$

where N is the local buoyancy frequency. As discussed in Blumberg *et al.* (1992), in one dimension (depth) the MY2.5 closure consists of evolution equations for vertically varying q^2 and $q^2 l$ that include terms representing production (sources), dissipation (sinks), and diffusion. These are supplemented by the stratification length scale limitation suggested by Galperin *et al.* (1988):

$$l \leq 0.53 q/N \tag{9}$$

which requires that the turbulence length scale be less than the Ozmidov scale, i.e. the supposed largest scale possible in stratified turbulence (Gregg, 1987). We have found that this length scale limitation significantly affects the calculated turbulence properties.

Since the tide is dominant in inducing vertical mixing in many shallow systems, especially during nonstorm conditions. our use of this model thus far has been confined to cases for which the interaction of the current with the bottom roughness is the primary source of turbulence; this study does not consider wind-induced mixing. Bottom friction is parameterized by specifying a bottom roughness (we use 1 cm) and assuming that U at the point closest to the bottom conforms to the law of the wall written in terms of the bottom roughness (Blumberg and Mellor, 1987).

The transport equations for salinity (Eq. 3), momentum (Eq. 5). q^2, and $q^2 l$ are solved on a staggered finite difference grid using the code described by Blumberg *et al.* (1992), hereinafter referred to as BGO. Turbulence quantities are used to update the momentum and salt fields (via ϵ_z and K_z), which in turn are used to update the turbulence fields. In our application the grid typically has 5 cm vertical resolution (much finer than what might be used with a full 3D circulation model). while the time ctep is usually 100 s or less. The resulting eddy diffusivities, used in the phytoplankton model runs discussed below. were calculated for SIPS flows and runaway stratification cases, as well as for constant stratification cases where the vertical density distribution is specified and the salinity evolution equation is omitted. The version of the model used for the first two types of flows we refer to as "BGO-SIPS," while the latter we refer to as "BGO-SPEC." Apropos to the discussion above. the use of the two different forms of the model allows us to represent a wide range of estuaries, albeit in a simplified fashion.

c. Results: Turbulent mixing coefficients and stratification

Depending on the relative strengths of the tidal current and the longitudinal density gradient, and thus the balance between tidal mixing and the stabilizing river flow, the results may display either tidally intermittent stratification (SIPS) or persistent (runaway) stratification (Monismith *et al.*, 1996). Figures 3a and 4a show BGO-SIPS' predicted distributions of K_z, the vertical turbulent diffusivity, in time (horizontal axis) and space (vertical axis) for a SIPS case and a runaway stratification case, respectively. Figures 3b and 4b display instantaneous K_z profiles for each case at different phases of the tidal cycle: Figures 3c and 4c show the top-bottom salinity difference (ΔS) versus time; and Figures 3d and 4d plot depth-averaged tidal velocity (U_{ave}) versus time for each case.

In the SIPS case (Fig. 3), attenuation of mixing in the upper water column and an overall increase in ΔS is seen in each ebb/early flood period. By mid-flood. however. mixing and reverse straining are strong enough to begin to erode the stratification, producing the observed decrease in vertical salinity difference. During mid-ebb. tidal mixing is enough to partially homogenize the salinity profile, resulting in a temporary decrease in ΔS. For the runaway stratification case (Fig. 4), mixing in the upper water column is conctantly attenuated by the pycnocline (once the permanent stratification forms), and the vertical salinity difference grows with time. Nonetheless, a semidiurnal signal can still be seen in the vertical salinity difference, indicating that gravitationally induced runaway stratification and SIPS can act concurrently.

The SIPS case (Fig. 3) is typical of lagoonal systems like south San Francisco Bay where, except in very wet years (e.g. 1995). the influence of freshwater is relatively weak and tidal mixing is usually able to destroy any temporary stratification which may form. On the other hand. the runaway stratification case (Fig. 4) is typical of strongly stratified estuaries such as north San Francisco Bay during the spring, where freshwater flow through the Sacramento-San Joaquin Delta may generate a strong longitudinal density gradient which dominates tidal mixing (Monismith *et al.*, 1996). Actual data (Fig. 2) show ΔS ultimately declining after a runaway stratification event due to the increase in U_{max} (tidal forcing) as a spring tide is approached, resulting in a breakdown of the runaway stratification. In the simulations discussed in this paper, U_{max} is constant; therefore, variation over a spring-neap cycle is not explicitly modeled.

d. Summary and caveats

The system of equations we present above represents a minimal description of the physics of estuary flows in general and is the unsteady counterpart to the analysis of subtidal flows given originally by Hansen and Rattray (1965). They showed the existence of a core region of a partially mixed estuary in which advective accelerations were negligible and the resulting salinity field varies approximately linearly with distance along the axis of the estuary. Observational evidence for this type of salinity field is given in Jassby *et al.* (1995) who showed self-similar distributions of salinity in northern San Francisco Bay in which the salinity varied linearly over a large part of the estuary

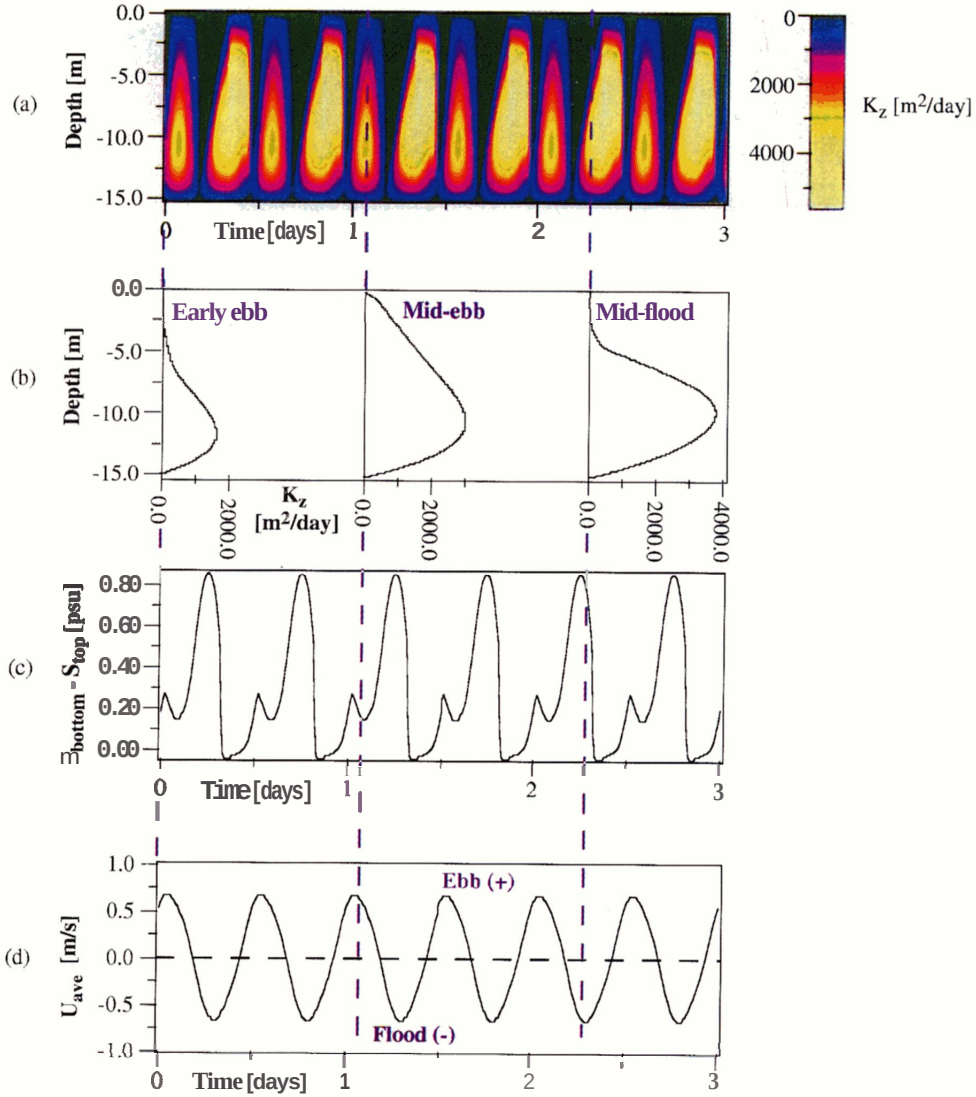

Figure 3. (a) Turbulent diffusivity time series, (b) instantaneous profiles of turbulent diffusivity, and timeseries of (c) vertical salinity difference and (d) depth-averaged tidal velocity for a SIPS case; predicted by BGO-SIPS.

downstream of the upstream limit of salinity intrusion. It is the local perturbation of this mean salinity field, effectively maintained by a balance of **subtidal** processes, that we solve for with our model. Thus, while our model omits important physical processes like **frontogenesis** (see, **e.g. O'Donnell,** 1993) with concomitant effects on phytoplankton transport **(e.g.** Franks and Chen, **1996),** it does represent a first-order description of vertical

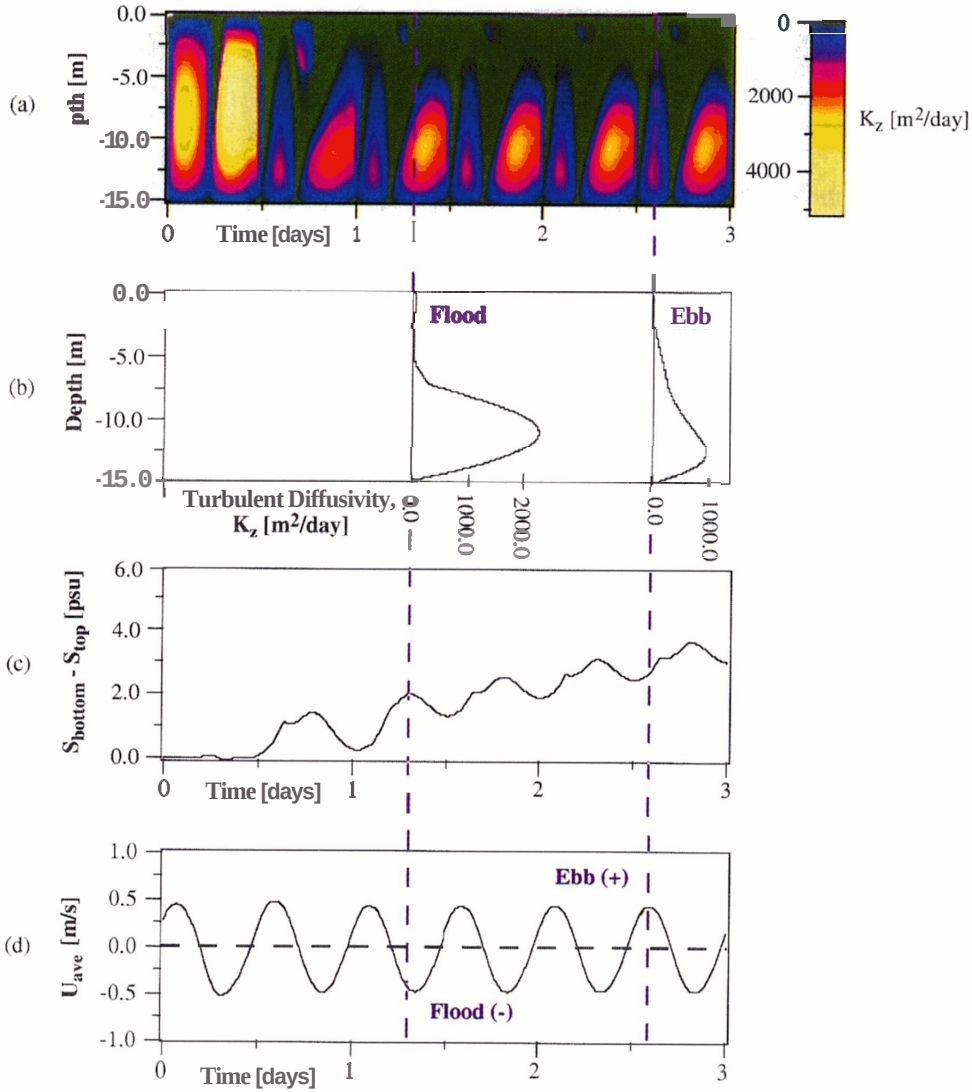

Figure 4. (a) Turbulent diffusivity timeseries, (b) instantaneous profiles of turbulent diffusivity, and tirneseries of (c) vertical salinity difference and (d) depth-averaged tidal velocity for a runaway stratification case; predicted by BGO-SIPS.

mixing in the stratified tidal channels that can be found in many coastal plain estuaries like San Francisco Bay or the James River.

In our approach we have neglected the vertical velocity w, which we justify as follows. In our simulations, the rising and falling of the water surface throughout the tidal cycle are not modeled: instead the grid is fixed. In a barotropic tide, w can be scaled as $w \approx (\partial H/\partial t)(1 + z/H)$, where z is the local depth and H is the total depth. If we assume that the

depth varies periodically as $H = H_0 + A\sin[2\pi^* t/T]$, where T is the period of motions (—12.4 hours) and A is the amplitude of tidal motions, then w is at most $[2\pi^* A/T]$. If A is about 1 m (e.g. for San Francisco Bay), then vertical velocities are about 0.15 mm/s, which is quite small. Therefore, we argue that the vertical velocities induced by the tide are not significant in light of other approximations we have made in constructing the model. This picture certainly will change for flows in several dimensions where features like fronts can induce significant vertical velocities.

Most importantly. this idealization allows us to generate turbulent mixing results like those described above that reflect different forms of stratification, i.e., persistent or intermittent. In either case, it is important to bear in mind that vertical mixing in stratified estuaries results primarily from two sources of turbulence production if wind is neglected: the bottom boundary layer and shear that is internal to the water column (Abraham. 1988; Monismith and Fong, 1996). As we will demonstrate below, this is important to phytoplankton dynamics because bottom-generated turbulence produces a bottom mixed layer that entrains fluid from above as it grows. This results in phytoplankton cells being mixed from the photic zone (if it is shallow) and circulated over the deeper (and hence darker) part of the water column. This is different from the case found in lakes or in the ocean where mixed layer deepening involves entraining fluid from below. hence retaining cells in the upper mixed layer, though reducing the average light exposure of those cells. In later sections. we will show that this difference is important to understanding why the details of the stratification matter to estuarine phytoplankton dynamics.

3. The biological system

a. Phytoplankton dynamics

In the type of system we are examining (i.e. shallow, with substantial tidally generated turbulent kinetic energy). turbidity (Cloern. 1987) and benthic grazing (Cloern. 1982: Herman, 1993) may control phytoplankton bloom initiation. In addition. zooplankton grazing. sinking of the phytoplankton, and respiration losses can also influence bloom development. Our phytoplankton model incorporates all of these factors. The current formulation does not, however, account for nutrient dependence/availability since, in many estuaries (e.g. south San Francisco Bay). nutrients are more pertinent to bloom termination than initiation.

The phytoplankton model is not calibrated or "tuned": rather, it is based upon standard forms of equations for scalar transport and phytoplankton growth and employs parameter values representative of field measurements. Because south San Francisco Bay (SSFB) has been the source of detailed biological records over the last two decades (Cloern, 19961, this system serves as our "laboratory" for investigating phytoplankton dynamics in shallow estuaries. Thus, the parameter ranges used in our model (e.g. depths, benthic grazing rates. light attenuation coefficients. and rates of sinking, zooplankton grazing, and respiration) are typical of SSFB.

b. The phytoplankton model

The phytoplankton model is based upon a time- and depth-dependent advection-diffusion equation for transport, sources, and sinks of phytoplankton biomass in a one-dimensional vertical estuarine water column. Thus, the phytoplankton model has been named "V1D." This configuration is based on the assumption that the conditions relating to vertical transport and net phytoplankton growth rates are horizontally homogeneous. The general model equation is:

$$\frac{\partial B}{\partial t} = \mu_{net} B + \frac{\partial}{\partial z}\left(K_z \frac{\partial B}{\partial z}\right) - \frac{\partial}{\partial z}(W_s B) - \frac{\partial}{\partial z}(\alpha B) \tag{10}$$

where B is the phytoplankton biomass measured as chlorophyll *a* [mg chl *a*/m^3]; μ_{net} is the net rate of biomass growth [d^{-1}] (gross growth rate minus losses to respiration and zooplankton grazing); K_z is the vertical turbulent diffusivity [m^2/d] (see Section 2b for details); W, is the phytoplankton sinking rate [m/d]; and α is the benthic grazing rate [m^3/(m^2-d)], which is nonzero only at the bottom boundary. The phytoplankton growth rate is calculated using Jassby and Platt's (1976) hyperbolic tangent function for productivity, a constant ratio of phytoplankton cellular carbon to chlorophyll, and an exponentially decaying irsadiance with depth. Values typical of SSPB are used for maximum growth rate, respiration rate. zooplankton grazing rate, average daily surface irradiance, sediment-related light attenuation, benthic grazing rate, and sinking speed, which are all taken to be constant in time (see Table 1, Koseff *et al.* (1993), and Appendix for details).

The current version of V1D is based upon the model developed by Cloern (1991) and later refined by Koseff *et al.* (1993). However, instead of a finite difference formulation, this version uses a finite volume approach (MacCormack and Paullay, 1972), which is mass-conservative and greatly simplifies implementation of flux boundary conditions. The model employs a staggered grid which is divided into control volumes, or cells (Fig. 5*)*. On this grid, B and μ_{net} (biomass and sources/sinks) are defined at cell centers, while K_z and W_s (all flux-related quantities) are defined at cell faces. In this manner, we can enforce mass conservation, i.e. that for a given control volume:

(Sources + Inward Fluxes) − (Sinks + Outward Fluxes) = Accumulation

With this finite volume/staggered grid approach in solving the mass transport equation, mass is conserved to within (at least) 10^{-6} [mg chl *a*/m^3]. Since domain boundaries coincide with cell faces, where fluxes are defined, any zero flux terms on the boundaries fall out of the discretization for the boundary cells, making "phantom" points outside of the flow domain unnecessary. We have applied Leonard's (1979) QUICK (Quadratic Upstream Interpolation for Convective Kinematics) scheme to the advective terms, which are treated explicitly in time. The turbulent diffusion terms are central differenced and treated implicitly in time. Growth and benthic grazing terms are treated implicitly, as well. (See Appendix for more details on the numerical formulation.)

Table I. Variables and constants relevant to models and results.

Name	Units	Value/ range	Description
a	m^2-d/Einst.	0.1	Photosynthetic efficiency at low irradiance
$B(z, t)$	mg chl a/m^3		Phytoplankton biomass
$\overline{B}_5$	mg chl a/m^3		Depth-averaged biomass at t 5 days
$\overline{B}^{sl}$	mg chl a/m^3		Surface layer averaged biomass
$\overline{B}^{sl}_5$	mg chl a/m^3		Surface layer averaged biomass at $t = 5$ days
Flux out	mg chl a		Total biomass lost from surface layer over one timestep
F_{turb}	mg chl a		Biomass lost from surface layer via turbulent mixing over one timestep
H	m	15. 165	Water column height
$I(0)$	Einst /(m^2-d)	40	Mean daily suri'ace irradiance
$I(z, t)$	Einst /(m^2-d)		Photosynthetically active radiation
$K_z(z, t)$	m^2/d		Vertical turbulent diffusivity
$K^{sl}_{z_{max}}$	m^2/d		Maximum turbulent diffusivity in surface layer
K^{int}_z	m^2/d		Turbulent diffusivity at bottom of surface layer
$k_b(z, t)$	1/m		Light attenuation by phytoplankton
k_t	1/m	*0 5–30 0*	Abiotic light attenuation coefficient
l	m		Turbulence lengthscale
$P(z, t)$	mg C/(mg chl a-d)		Phytoplankton c assimilation rate
Pe_t			Turbulent Peclet number
P_{max}	mg C/(mg chl a-d)	100	Maximum phytoplankton c assimilation rate
Prod	mg chl a		Net biomass production in surface layer over one timestep
P^{sl*}_{net}			Net accumulation of biomass in surface layer over one timestep normalized by surface layer production
q^2	m^2/s^2		Turbulent kinetic energy
r		0.05	Respiration rate (fraction of P_{max})
S	psu		Salinity
t	d		Time
T_{pyc}	m	0.5–8	Thickness of pycnocline
U_{max}	m/s	0.5–1.5	Maximum tidal current velocity
W_s	m/d	0–5	Phytoplankton sinking rate
x	km		Longitudinal (streamwise) distance
z	m		Depth
Z_{cr}	m		Critical depth
Z_m	m	0–15	Surface layer depth
ZP	1/d	0.1	Zooplankton grazing rate
α	m^3/(m^2-d)	0–15	Benthic grazing rate
β	1/psu		Coefficient of saline expansivity
ΔS	psu	0–10	Vertical salinity difference
Δt	d	0.0005	Timestep
Δz	m	0.05	Grid spacing
Γ	psu/km	0.0–0.3	Longitudinal salinity gradient ($\partial S/\partial x$)
$\mu_{net}(z, t)$	1/d		Net phytoplankton growth rate
$\overline{\mu}^{sl}_{net}$	1/d		Surface layer averaged net growth rate
θ	mg C/mg chl a	50	Ratio of cellular carbon to chlorophyll
ρ	kg/m^3		Water density

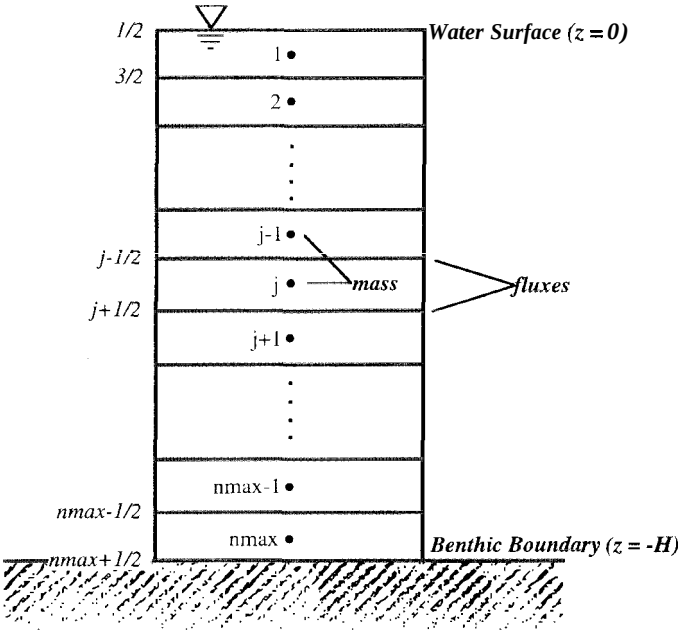

Figure 5. Computational grid for V1D, the one-dimensional phytoplankton model

4. Physical/biological coupling

a. The general *effects of periodic* and persistent *stratification on phytoplankton* dynamics

In this section, we compare the effects of periodic and persistent stratification on phytoplankton bloom initiation. We used BGO-SIPS to simulate a 15 m deep water column for various longitudinal salinity gradient ($\partial S/\partial x$) and tidal forcing (U_{max}) conditions. Each case depicts a particular balance between tidal mixing and river flow. A depth of 15 m was chosen because it is typical of the channel in south San Francisco Bay. These hydrodynamic simulations were used to provide the turbulent mixing information (K_z's) for the phytoplankton model (V1D), in which we varied the light attenuation and benthic grazing strength. Overall, we note the following: (1) Tidally intermittent stratification (SIPS) does not increase the likelihood of a bloom beyond that of a constantly unstratified water column; (2) Persistent stratification significantly increases the probability of a bloom for a range of light attenuation and benthic grazing conditions.

These results are illustrated in Figure 6 (and associated Table 2), which shows a sample set of bloom threshold curves as a function of light attenuation (k_t) and benthic grazing rate ***(a)***. Each curve represents a unique combination of hydrodynamic conditions which are described in Table 2. For each point on each curve, several V1D simulations were performed (each with a different k_t) to iteratively find a k, value which just allows a bloom. For all curves, the phytoplankton sinking rate is $W_s = 0.5$ m/d. Abiotic light attenuation and benthic grazing rate were chosen as the independent variables because they each have

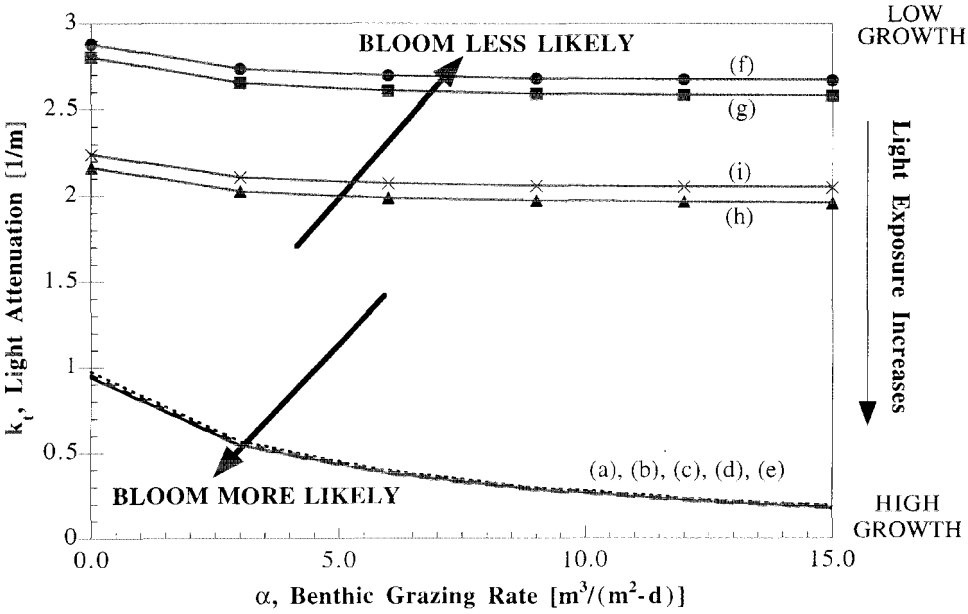

Figure 6. Light attcnuation-benthic grazing bloom threshold curves for 1D 15 m deep water column. Description of the hydrodynamic case associated wiih each curve is in Table 2.

the potential to control net phytoplankton population growth in the water column and may vary widely over time. At first glance, the combination of k_t and α on the same plot may seem peculiar since, in the field. k, may vary on timescales of minutes to hours, while α may vary on timescales of weeks. However, in the phytoplankton simulations performed with V1D, k, is taken to be an average value of light attenuation over timescales of days.

In Figure 6, the x-axis is proportional to the sink term (benthic grazing). and the y-axis increases inversely with the source term (light-driven production). Thus, as a point departs from the origin, grazing losses increase and mean light exposure decreases, thus diminish-

Table 2. Describes cases associated with curves in Figure 6. "Hydrodynamic Code" describes version of RGO used to calculate turbulent diffusivities for that case.

I D.	Hydrodynamic code	Stratification behavior	$\partial S/\partial x$ [psu/km]	U_{ma}, [m/s]	H [m]	Z_m [m]
a	BGO-SIPS	Unstratified	0.000	0.60	15.0	—
b	BGO-SIPS	Unstratified	0.000	0.90	15.0	—
c	BGO-SIPS	Periodic	0.065	0.60	15.0	—
d	BGO-SIPS	Periodic	0.065	0.90	15.0	—
e	BGO-SIPS	Periodic	0.261	0.90	15.0	—
f	RGO-SIPS	Persistent	0.261	0.60	15.0	1.1
g	BGO-SIPS	Persistent	0.147	0.50	15.0	1.3
h	BGO-SIPS	Persistent	0.196	0.50	15.0	2.4
	BGO-SIPS	Persistent	0.261	0.50	15.0	2.2

ing the likelihood of a bloom. The curves bound the conditions under which blooms will likely occur: for k_t-α conditions producing a point above a particular curve, a bloom will not occur for the hydrodynamic case represented by the curve; whereas conditions producing points below the curve indicate that a bloom will occur for that hydrodynamic case. These threshold curves thus demonstrate how physical processes influence the balance between light-driven production and grazing losses. For example, Curve 'd'. which corresponds to $\partial S/\partial x$ = 0.065 psu/km and U_{max} = 0.9 m/s (an intermittent stratification case) is indicated by the "- - -" line. If the benthic grazing rate is 5 $m^3/(m^2–d)$, then in order for a bloom to occur the light attenuation must be less than 0.5 m^{-1} (a condition extremely rare in SSFB). However, Curve 'i' shows that if $\partial S/\partial x$ = 0.261 psu/km and U_{max} = 0.5 /ms (a runaway stratification case), for similar benthic grazing conditions (5 $m^3/(m^2–d)$) the light attenuation can be as high as 2.1 m^{-1} (a condition common in SSFB) and a bloom will still occur.

The following points emerge from examination of Figure 6. First. the phytoplankton model predicts that for a 15 m deep water column, extremely clear water is necessary to produce a bloom for tidally intermittent stratification (SIPS). as well as for the constantly unstratified case ($\partial S/\partial x$ = 0), even with zero benthic grazing. In fact. the bloom threshold curves for the tidally intermittent stratification case essentially overlay those for the constantly unstratified case, suggesting that the SlPS mechanism does not increase the likelihood of a bloom beyond that of a constantly unstratified water column. This trend is attributable to the fact that in the unstratified and SlPS cases mixing of the phytoplankton down through the water column is faster, on average, than their growth. Second, it is evident that runaway stratification allows a bloom to occur under much more turbid conditions than in the unstratilied and SIPS cases. Runaway stratification lengthens the timescale for vertical transport of the phytoplankton relative to the timescale for growth, allowing the phytoplankton to remain in the upper water column (photic zone) long enough to multiply. Third, the intermittent stratification and unstratified threshold curves exhibit steeper overall slopes than the runaway stratification cases. indicating, as expected (Cloern, 1991), that the effects of benthic grazing on an unstratified or intermittently stratified water column are more marked than on a persistently stratified water column.

Under runaway stratification conditions, a vertical density structure similar to that sketched in Figure 7a may develop. Different runaway stratification cases may exhibit different values of surface layer depth, or Z_m. As evidence of the general structure shown in Figure 7a, Figure 7b shows field measurements of salinity and chlorophyll concentrations corresponding to the large runaway stratification event in SSFB depicted in Figure *2*. The surface layer and a pycnocline at ~5.5 m depth are obvious in the field data, as is the effect of the pycnocline on the phytoplankton (i.e. inhibition of downward transport).

For each runaway stratification case plotted in Figure 6, the estimated value of Z_m is listed in Table 2 alongside the corresponding $\partial S/\partial x$, U_{max}, and H values. For the unstratified and periodically stratified cases, the pycnocline is either absent or not persistent and so is represented as "—" in the Z_m column. Notice that the curves (e.g., 'h', 'i') in Figure 6 appear to be grouped by values of Z_m, with a significant distance between groupings. In

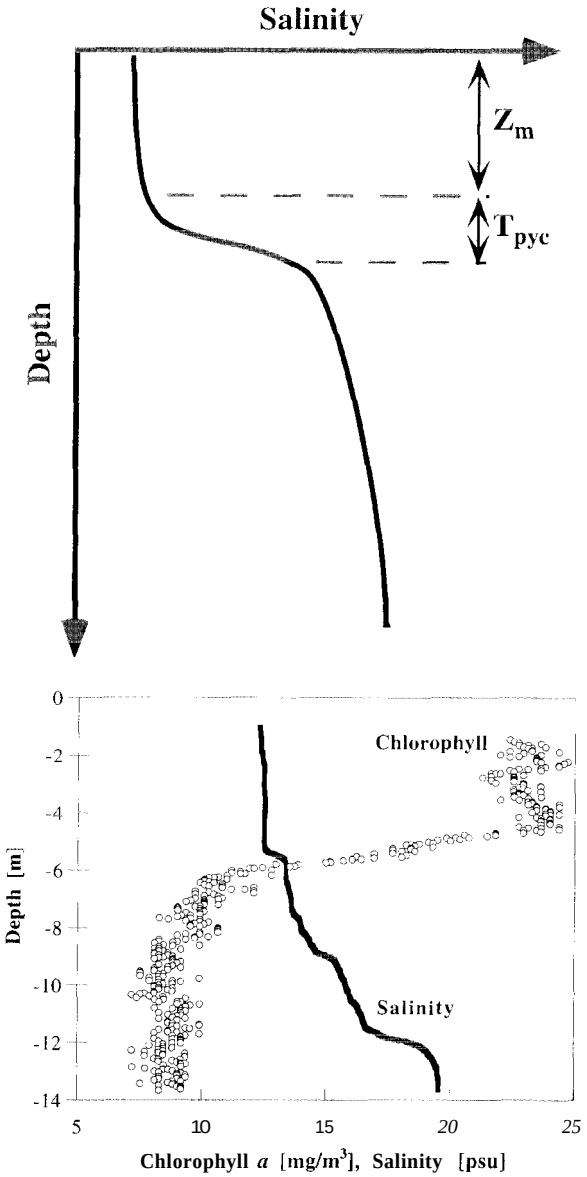

Figure 7. (a). Typical vertical salinity profile when runaway stratification forms. (b) Instantaneous vertical salinity and chlorophyll profiles at San Mateo Bridge, south San Francisco Bay. on April 11, 1995. Data from Edmunds *et al.* (1997).

these cases, a shallower mixed layer is more likely to produce a bloom. This indicates that, in addition to the issue of intermittency versus persistence of stratification, other details of the stratification are important to the phytoplankton dynamics as well. We explore these details of the stratification below.

b. Applicability of the critical depth model to shallow estuaries

i. *Background.* In the previous section, we discussed the general effects of periodic and persistent stratification on phytoplankton bloom dynamics. Whereas persistent stratification may significantly increase the likelihood of a bloom relative to an unstratified water column, periodic stratification (SIPS) does not. Furthermore, for the persistent stratification cases, the surface layer depth. Z_m, appears to influence the bloom threshold curves in Figure 6. In this section, we explore the applicability of Sverdrup's Critical Depth Model (SCUM) to estuarine systems in predicting the onset of phytoplankton blooms. We used the VID phytoplankton model with the modified BGO hydrodynamic model to explore the effects of the details of persistent stratification and vertical transport on bloom dynamics and to answer Questions 2 and 3 posed in the introduction.

ii. *Approach.* A modified BGO model was used to generate vertical turbulent diffusivity fields associated with different scenarios of persistent stratification. In persistent stratification cases simulated by BGO-SIPS (which allows the stratification to evolve from a balance between the oscillating tidal pressure gradient and a longitudinal density gradient), we can neither predict nor directly control the stratification characteristics such as Z_m, T_{pyc} (the thickness of the pycnocline), or AS (the vertical salinity difference). Therefore, we developed BGO-SPEC, which allows us to specify the stratification parameters for each run, hold them constant, and subject the water column to an oscillating tidal current. This enables us to explore the relationship between Z_m (and T_{pyc}, AS) and bloom initiation in a controlled fashion.

Holding the stratification parameters constant (to emulate a constant source of buoyancy) is not completely realisiic; however, as is shown in Figure 8. this method produces a reasonable approximation to the effects of the physics, as modeled by BGO-SIPS, on the phytoplankton. In Figure 8, k_t-α bloom threshold curves are shown for a range of runaway stratification conditions generated by BGO-SIPS and by BGO-SPEC. The hydrodynamic parameters for all cases are summarized in Table 3. For each BGO-SIPS case, we averaged the resultant stratification parameters over the run and then used those average values for Z_m, T_{pyc}, and ΔS in the associated BGO-SPEC run. The k_t-α threshold curves generated by VID for each pair of cases are very close. For example. Case 'a'. for which $\partial S/\partial x = 0.131$ psu/km and $U_{max} = 0.47$ m/s, resulted in an average Z_m of 0.7 m, $T_{pyc} = 0.8$ m, and $\Delta S = 1.7$ psu. For this particular case, the maximum light attenuation allowing a bloom (for $\alpha = 0$) is about 3.4 m^{-1}. A separate BGO-SPEC simulation using the average stratification parameters and holding them fixed (Case 'b') resulted in a maximum light attenuation for a bloom of about 3.7 m^{-1}. Even closer correspondence is evident in the other cases. For example, the maximum light attenuation for the BGO-SIPS Case 'e' ($k_t = 1.66\ m^{-1}$) is exceptionally close to that for the associated BGO-SPEC scenario, Case 'f' ($k_t = 1.69\ m^{-1}$). This type of comparison assures us that BGO-SPEC provides a sound approach for exploring the effects of Z_m on bloom initiation.

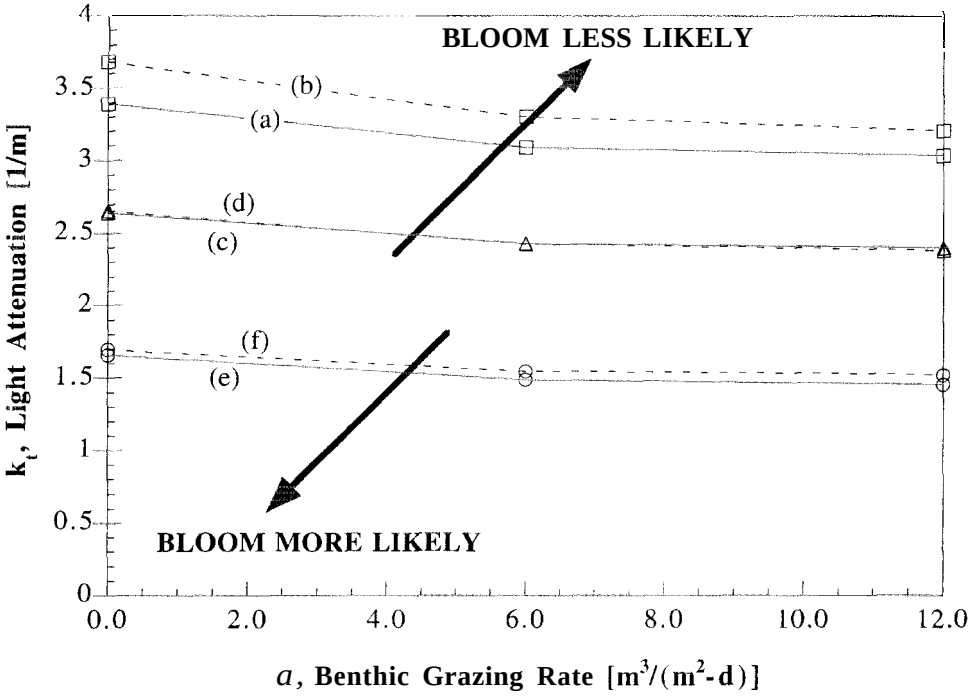

Figure 8. Light attenuation-benthic grazing thresholds comparing SIPS-derived cases (using BGO-SIPS) to fixed-pycnocline cases (using BGO-SPEC). Each pair shares the same symbol; the solid line is for the BGO-SIPS case; the dashed line is for the associated BGO-SPEC case. Description of the hydrodynamic case associated with each curve is in Table 3.

iii. Relationship of surface layer depth to bloom inception and nzagnitude. V1D and BGO-SPEC enabled us to explore the effects of surface-layer depth on bloom initiation and, in particular, the applicability of the SCDM to shallow estuarine systems. We did this by calculating phytoplankton population growth for different ratios of surface layer depth to critical depth and then comparing model results with the SCUM criterion that growth is

Table 3. Describes cases associated with curves in Figure 8. "Hydrodynamic Code" describes version of BGO used to calculate turbulent diffusivities for that case. For BGO-SIPS cases, Z_m, T_{pyc}, AS are time-averaged values.

I.D.	Hydrodynamic code	Stratification behavior	$\partial S/\partial x$ [psu/km]	U_{max} [m/s]	H [m]	Z_m [m]	T_{pyc} [m]	ΔS [psu]
a	BGO-SIPS	Persistent	0.131	0.47	15.0	0.70	0.8	1.7
b	BGO-SPEC	Persistent	—	0.47	15.0	0.70	0.8	1.7
c	BGO-SIPS	Persistent	0.261	0.69	15.0	1.75	0.6	10.0
d	BGO-SPEC	Persistent	—	0.69	15.0	1.75	0.6	10.0
e	BGO-SIPS	Persistent	0.261	0.75	16.5	4.00	0.7	8.5
f	BGO-SPEC	Persistent	—	0.75	16.5	4.00	0.7	8.5

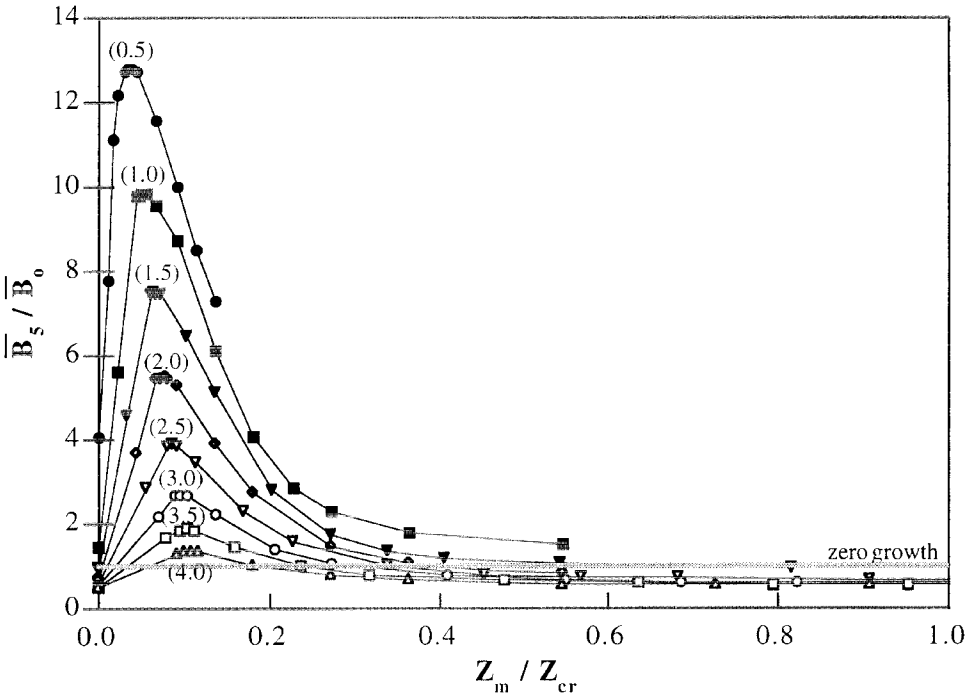

Figure 9. Depth-averaged phytoplankton biomass at $t = 5$ days normalized by initial average biomass versus ratio of surface layer depth to critical depth. Next to each curve is the value of light attenuation coefficient in [m^{-1}] associated with that curve. Also shown is a line representing rate of zero growth per day. For all data, $H = 15$ m, $U_{max} = 0.75$ m/s, $T_{pyc} = 1$ m, $\Delta S = 5$ psu, $W_s = 0.5$ m/d, and $\alpha = 0$ $m^3/(m^2\text{–d})$.

positive (blooms occur) whenever $Z_m/Z_{cr} < 1$. To this end, we show calculated $\overline{B_5}$, the depth-averaged phytoplankton biomass at $t = 5$ days, normalized by $\overline{B_o}$, the initial average concentration (3 mg chl a/m^3), plotted versus Z_m/Z_{cr} for a range of light attenuation values (Fig. 9). For all these cases, $H = 15$ m, $U_{max} = 0.75$ m/s, $T_{pyc} = 1$ m, $\Delta S = 5$ psu, $W_s = 0.5$ m/d, $\alpha = 0$ $m^3/(m^2\text{–d})$, and the maximum growth rate $\mu_{max} = 2$ d^{-1}. The simulation length of five days was chosen because it is representative of the typical duration of persistent stratification in a system for which spring/neap mixing effects are significant (see Fig. 2). Z_{cr} is calculated as the depth at which the integral net growth rate (see Appendix, Jassby and Platt, 1976), including the effects of respiration, zooplankton grazing, and depth-variable irradiance (neglecting self-shading), is zero. Each curve is the result of several five-day phytoplankton simulations with V1D, which used turbulent diffusivities generated by BGO-SPEC. For each curve, abiotic light attenuation (k_t) is held constant and only Z_m varies. We produced curves for different light attenuation values because k_t essentially sets Z_{cr} (each curve is therefore associated with a particular Z_{cr}). If the SCDM captures the processes controlling bloom development and collapses them into one

universal relationship, then the applicability of the SCDM should be independent of Z_{cr} (i.e. all the curves in Figure 9, which differ only by Z_{cr}, should display the same behavior with respect to bloom initiation).

From the perspective of maximizing phytoplankton production, it is evident that for each k_t there is an "optimal" pycnocline depth, at which the peak of each curve is located. For points on either side of the peak, conditions are less than optimal such that the biomass produced in the water column is less than the maximum. Also plotted in Figure 9 is a horizontal line representing zero growth in depth-averaged phytoplankton biomass. It is evident that there are numerous cases for which $Z_m/Z_{cr} < 1$ but population growth is negative. Because the traditional critical depth model applies to surface layer averaged biomass rather than depth-averaged biomass, we checked the cases with $Z_m/Z_{cr} < 1$ that fell below the zero-growth level and confirmed that in the majority of those cases surface layer averaged biomass did not increase either. Model results are therefore inconsistent with the traditional SCDM. Specifically, our results indicate the following for the systems considered here: (1) $Z_m/Z_{cr} = 1$ does not provide a "switch," below which there is biomass increase; (2) There appears to be no such "switch" for predicting blooms since, for any one value of Z_m/Z_{cr}, there are numerous possible depth-averaged (and surface layer averaged) biomass values, some which may be considered a bloom and some which may not; (3) The traditional "critical depth" concept therefore must not capture all of the crucial processes controlling bloom initiation in a stratified estuarine water column.

As we show below, the process missing from the classical SCDM is leakage of phytoplankton from the surface layer via sinking and turbulent mixing. First, however, we explain the unexpected non-monotonic behavior of the curves in Figure 9.

c. *Origin of the non-monotonic relation between population growth and mixed-layer depth*

The SCDM implies that phytoplankton population growth increases as Z_m decreases, and Riley (1942) suggested a simple monotonic relationship based upon measurements in Georges Bank. The nonmonotonic relationship between simulated phytoplankton biomass growth and surface layer depth in Figure 9, however, shows that shallower is not necessarily "better," with respect to phytoplankton bloom initiation. Four physical and biological processes are influenced by Z_m and will be considered as a basis for explaining Figure 9.

i. Turbulent mixing. The surface layer depth, Z_m, is closely associated with the intensity of turbulent mixing in the surface layer and thus with the balance between mixing and sinking in the upper water column. The turbulent diffusivities (K_z's) calculated in BGO are proportional to ql, where q is the square root of the turbulent kinetic energy (TKE) and l is the turbulence macroscale (i.e. a typical eddy lengthscale, or scale over which phytoplankton cells are mixed by the turbulence). K_z profiles were calculated by BGO-SPEC for three values of Z_m but the same U_{max}, T_{pyc}, and ΔS (Fig. 10). Notice that for smaller Z_m, the

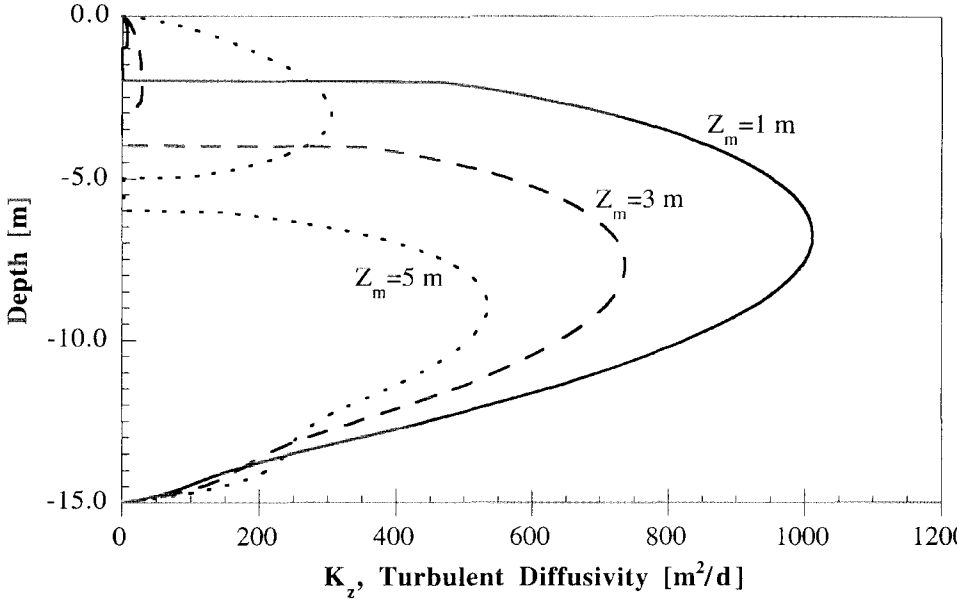

Figure 10. Turbulent diffusivity profiles predicted by the BGO-SPEC model for three different surface layer depths (Z_m). For all cases, T_{pyc} = 1 m, U_{max} = 0.75 m/s, and ΔS = 5 psu.

maximum turbulent diffusivity in the surface layer ($K_{z_{max}}^{s,l}$) is much smaller than for larger Z_m. As Z_m increases, the typical turbulent lengthscale for the surface layer increases, thus increasing K_z, which is proportional to l. An increase in l also indirectly (and nonlinearly) influences K_z by increasing shear production and turbulent transport of TKE up through the surface layer. These sources of TKE enhancement in the surface layer, as well as decreased dissipation of TKE (which scales as q^3/l), all contribute to higher K_z's in the surface layer as it is deepened. Furthermore, enhanced surface layer mixing is associated with greater turbulent diffusivities at the surface layer/pycnocline interface. Thus, for thicker surface layers, there is more turbulent leakage of phytoplankton out of the surface layer.

ii. Sinking in the presence of turbulent mixing. Mixing in the surface layer can be especially important to bloom dynamics when phytoplankton sink. If mixing is strong enough, it partially counteracts the sinking loss of phytoplankton from the surface layer. The balance between turbulent mixing and sinking can be represented by the turbulent Peclet number, the ratio of the mixing timescale to the sinking timescale:

$$Pe_t = \frac{\tau_{mix}}{\tau_{sink}} \sim \frac{L^2/K_z}{L/W_s} = \frac{LW_s}{K_z} \tag{11}$$

where L is the pertinent length scale (Z_m for the surface layer, for example), and K_z is the typical (e.g. average) turbulent diffusivity for the region of interest. If $Pe_t \gg 1$, sinking is

the dominant transport mechanism, and mixing is very slow by comparison. This case may be conceptualized by a group of quickly sinking particles, with turbulent mixing merely causing diffusion about the constantly sinking center of mass. If $Pe_z \ll 1$, turbulent mixing is the dominant transport mechanism, and sinking is very slow by comparison. This case may be conceptualized by a group of slowly sinking particles which are frequently transported upward by large. energetic turbulent eddies, resulting in a uniform vertical distribution of particles. If Pe_t is $O(1)$, mixing and sinking are equally significant transport processes.

If we consider the turbulent diffusivity profiles shown in Figure 10 for a particular combination of U_{max}, ΔS, and T_{pyc}, the typical turbulent diffusivities in the surface layer for Z_m = 1, 3, and 5 m are $O(1)$, $O(10)$, and $O(100)$ m^2/d, respectively. For a sinking velocity of $W_s = 0.5$ m/d, the turbulent Peclet numbers for ascending Z_m range from $O(1)$, for which sinking is important, to $O(0.01)$, for which sinking is relatively unimportant. Thus, larger Z_m values are associated with more intense surface layer mixing and, in turn, with lower turbulent Peclet numbers and, therefore, reduced sinking losses of phytoplankton from the surface layer. Platt *et al.* (1991) also suggested an inverse relationship between sinking-related losses and Z_m.

iii. Average net growth rate: Surface layer and below pycnocline. Surface layer depth controls bloom intensity in other ways. This is demonstrated in Figure 11, which shows two scenarios associated with different surface layer depths. Figure 11a is for a shallow surface layer, while Figure 11b is for a deeper surface layer. The shallow surface layer has less intense turbulent mixing, higher turbulent Peclet numbers, and, therefore, greater sinking losses than the deeper surface layer. However, the shallow surface layer has less turbulent leakage of phytoplankton than the deeper surface layer. The shaded area is the region of positive local net growth (where local growth rate exceeds respiration and zooplankton grazing losses). On the right. we show schematic vertical profiles of net growth rate and water density associated with each case. A smaller Z_m is associated with higher $\bar{\mu}^{sl}_{net}$, the average net growth rate over the surface layer (because mean light exposure of the surface layer phytoplankton increases as Z_m decreases).

Finally, depth-averaged biomass is affected by the net production that occurs below the surface layer. This subsurface phytoplankton is easily transported down by sinking while it is in the pycnocline region (since mixing there may be very weak) and by turbulent mixing below the pycnocline. In other words, if the depth at which local growth is zero extends below the surface layer (i.e. in the pycnocline or lower), phytoplankton will be produced that may be easily lost to the lower aphotic water column, as opposed to remaining longer in the surface layer, where it experiences positive net growth rates and is relatively isolated from benthic grazers. The significance of retaining cells in the region of maximal growth was emphasized by Smetacek and Passow (1990) as a key to bloom initiation.

The relationship of these four Z_m-related processes to the non-monotonic behavior of the curves in Figure 9 is illustrated further in Figure 12. This schematic of population growth

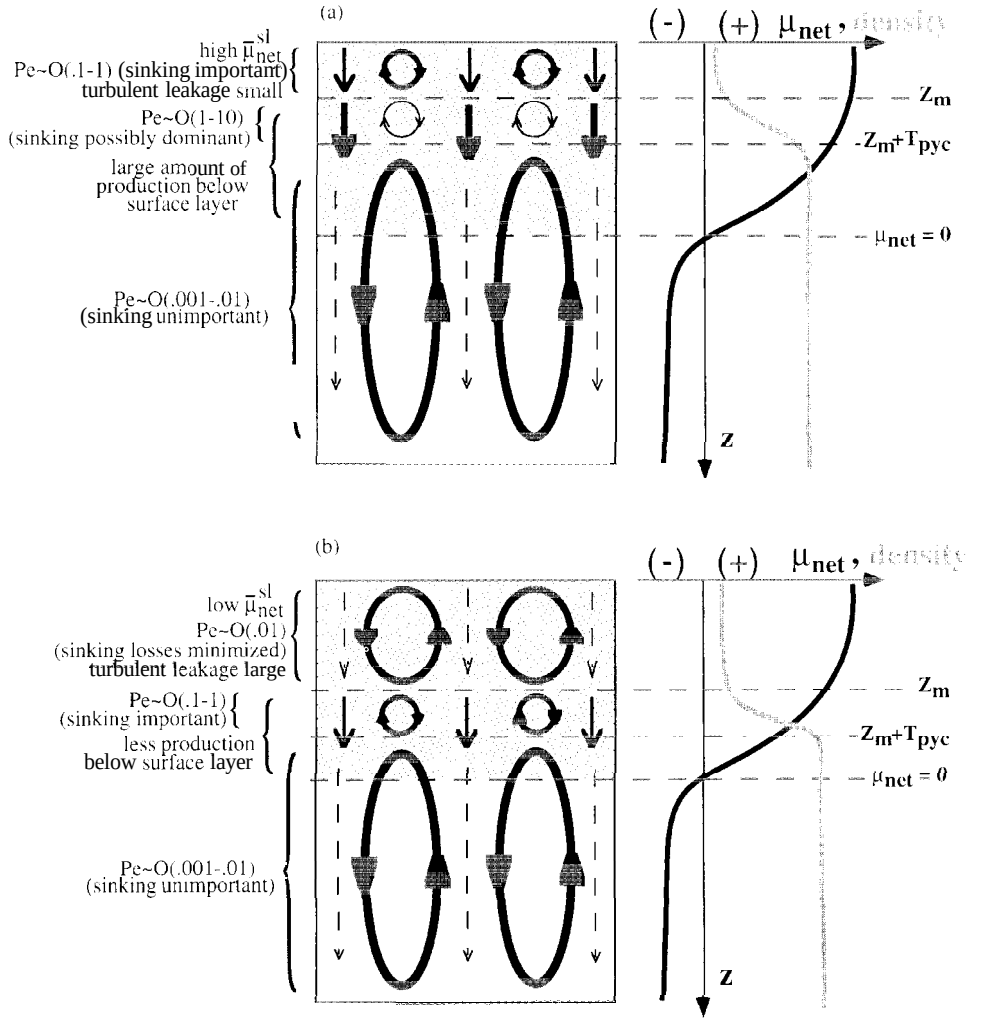

Figure 11. Water column schematics for two different scenarios: (a) a shallower surface layer and (b) a deeper surface layer. Arrows represent sinking and loops represent turbulent mixing; thickness of each connotes the relative strength. Shaded area of water column is the region of positive local net growth. On the r.h.s., corresponding sketches of net growth rate and density profiles are shown for each scenario.

(B_5/B_o) versus Z_m/Z_{cr} shows that for Z_m less than optimal (to the left of the peak), $\bar{\mu}^{sl}_{net}$ is large and turbulent leakage from the surface layer is minimized, but sinking losses may be significant and a large fraction of the production may occur below the surface layer. Opposite trends apply to Z_m values greater than optimal (to the right of the peak). The peak of the curve represents an optimal balance of these four conditions.

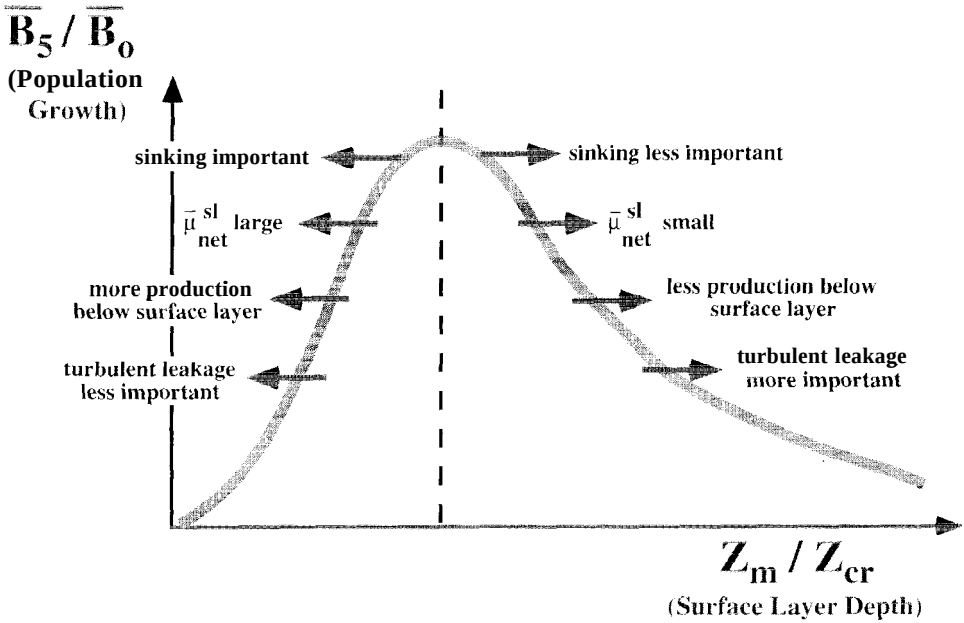

Figure 12. Schematic illustrating relationship between processes controlling bloom initiation and magnitude and surface layer depth. Z_m,.Explains non-monotonic behavior in Figure 9.

In Figure 13, we illustrate the diversity of functional relationships that can exist beiween phytoplankton population growth and mixed layer depth. The plot of $\overline{B_5}$, depth-averaged biomass at $t=5$ days, versus Z_m, is shown for both zero and nonzero sinking rates (Fig. 13a). Both relationships are nonmonotonic. This is because depth-averaged phytoplankton population growth is smaller when a large fraction of the produciion occurs below the surface layer. rather than solely in the surface layer. The $W_s = 0.5$ m/d curve shows that sinking augments the non-monotonic behavior. The plot in Figure 13b, on the other hand, shows B_5^{sl}, surface layer averaged phytoplankton biomass at $t = 5$ days, versus Z_m for zero and nonzero sinking rates. In the absence of sinking, $\overline{B_5^{sl}}$ decreases exponentially (i.e. monotonically) as Z_m, increases. Thus, if sinking is zero, the $\overline{B_5^{sl}}$–Z_m relationship is consistent with that proposed by Riley (1942). The reason for this is that surface layer averaged biomass is not affected by the production occurring below the surface layer. Therefore, if sinking is zero, then surface layer averaged biomass will decrease as Z_m, increases; whereas, if depth-averaged biomass is considered. or if sinking is nonzero. then there will be a non-monoionic relationship between surface layer depth and bloom intensity.

Note that the previous discussion is applicable to a purely tidally driven system. If wind is a significant source of TKE, the system will likely be less sensitive to sinking out of the surface layer because enhanced surface layer mixing would better counteract sinking (i.e., the turbulent Peclet number would be lower). Such a system would therefore tend to have a

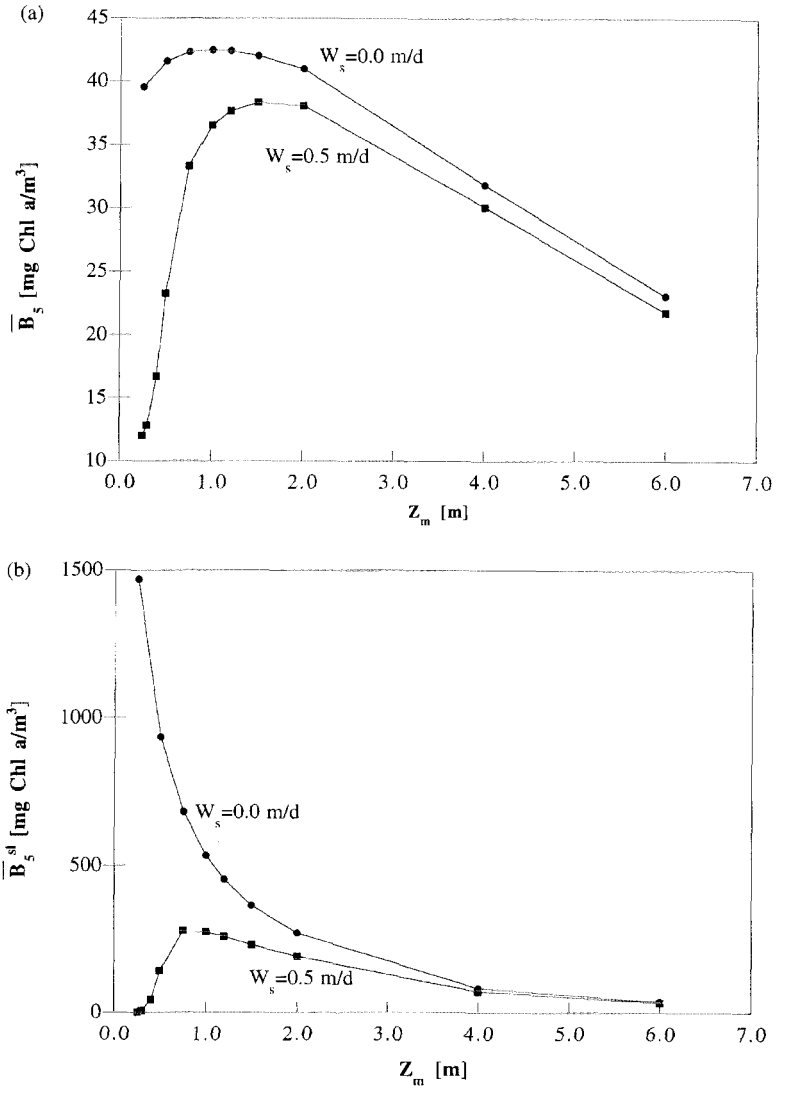

Figure 13. (a) depth-averaged phytoplankton biomass at t = 5 days and (b) surface layer averaged biomass at t = 5 days versus Z_m for zero and nonzero sinking speeds. For all cases, T_{pyc} = 1 m, ΔS = 5 psu, U_{max} = 0.75 m/s, H = 15 m, k_t = .5 m^{-1}, α = 0.0.

more monotonic relationship between depth-averaged phytoplankton biomass and surface layer depth. This relationship also depends on the function chosen to describe phytoplankton growth rate. For example, photoinhibition of algal growth (not included here) would suppress bloom development in very shallow surface layers, shifting the initial rise of the curve in Figure 12 toward the right.

Table 4. (a) $\overline{K_z^{int}}$, turbulent diffusivity at surface layer/pycnocline interface averaged over five days, for various combinations of Zm, U_{max}, T_{pyc}, and AS; for each such hydrodynamic case, two values of light attenuation, k,, were used; (b) $\overline{K_z^{int}}$ normalized by $\overline{K_z^{max}}$, the five-day average maximum turbulent diffusivity over the total water column depth; (c) the five-day average ratio of F_{turb}, the turbulent leakage flux from the surface layer, to Prod, the surface layer production, for the various hydrodynamic conditions as well as different values of k,. For all values in (c), W, = 0.0 and $\alpha = 0.0$

Z_m [m]	U_{max} [m/s]	T_{pyc} [m]	ΔS [psu]	k_t [m^{-1}]	(a) $\overline{K_z^{int}}$ [m^2/d]	(b) $\overline{K_z^{int}}/\overline{K_z^{max}}$ [−]	(c) $\overline{F_{turb}}$/Prod [−]
1	0.75	1	5	1	0.006	2.067E-06	0.036
				4			0.041
1	0.95	1	5	1	2.830	8.612E-04	0.821
				4			1.055
1	0.75	1	1	1	10.680	3.726E-03	0.913
				4			1.117
1	0.75	5	1	1	0.518	2.407E-04	0.514
				4			0.732
2	0.75	1	5	1	0.026	1.013E-05	0.059
				4			0.086
2	0.95	1	5	1	5.380	1.763E-03	0.802
				4			1.246
2	0.75	1	1	1	19.880	7.333E-03	0.899
				4			1.324
2	0.75	5	1	1	2.530	1.313E-03	0.627
				4			1.076

d. Leakage due to mixing

The previous section described sinking-induced leakage of phytoplankton out of the surface layer and, to a limited degree, leakage due to turbulent mixing. In this section, we elaborate on the effects of turbulent leakage which, as modeled, depends upon the turbulent diffusivities and phytoplankton concentration gradient at the interface between the bottom of the surface layer and the top of the pycnocline. These interfacial turbulent diffusivities are typically one or two orders of magnitude smaller than those characteristic of the inner surface layer and, in the case of very strong stratification, may be even smaller.

For a system in which the primary source of turbulence is the interaction of the current with the bottom roughness, the interfacial turbulent diffusivity, or K_z^{int}, generally increases as U_{max}, the maximum tidal current velocity, increases. Furthermore, since stratification inhibits the transport of turbulence up through the water column, K_z^{int} decreases with increasing AS and T_{pyc}. These relationships are demonstrated in Table 4, which shows values of time-averaged interfacial turbulent diffusivity, $\overline{K_z^{int}}$, predicted by *BGO-SPEC* for different combinations of Z_m, U_{max}, T_{pyc}, and ΔS. Also shown is the ratio of $\overline{K_z^{int}}$ to $\overline{K_z^{max}}$, the time-averaged maximum K_z over the depth. For each hydrodynamic case, the V1D phytoplankton model was used to simulate two scenarios, each for a different light

attenuation coefficient. For each phytoplankton simulation, two quantities were calculated: (1) F_{turb}, the turbulent leakage flux of phytoplankton from the surface layer over one timestep; and (2) Prod, the surface layer production over one timestep. Included in Table 4 is the time-averaged ratio of F_{turb} to Prod, or the average fraction of phytoplankton biomass produced in the surface layer that is lost via turbulent mixing.

The results in Table 4 show that. even for values of $\overline{K_z}^{int}$ which are 10^3–10^4 times smaller than the average maximum diffusivity, it is possible for the surface layer to lose 50% or more of its integral production via turbulent mixing. In fact. in more turbid water, phytoplankton growth rates may be so slow that turbulent mixing may remove more than 100% of what the surface layer produces (i.e. remove all of what was produced plus a portion of what existed previously). Thus, even "small" turbulent diffusivities can be responsible for significant losses of phytoplankton out of the surface layer. In the next section, we elaborate on the direct effects of surface layer leakage ---both advective and turbulent ---- on phytoplankton dynamics.

e. *The effects of leakage on phytoplankton blooms*

The reasons for the inapplicability of the traditional SCUM to shallow tidally driven systems become clear when we quantify the effects of surface layer leakage on blooms. Consider the quantity. P_{net}^{sl*}

$$P_{net}^{sl*} \quad \frac{\text{Prod} \quad \text{Flux out}}{\text{Prod}} \tag{12}$$

where:

$$\text{Prod} = \Delta t \int_{Z_{in}}^{0} \mu_{net} B dz$$

total net growth in surface layer over one timestep [mg chl a]

$$\text{Flux out} = \Delta t \left(-K_z \frac{\partial B}{\partial z} + W_s B \right)^{int}$$

total advective plus turbulent diffusive flux out of surface layer over one timestep [mg chl a]

(superscript "int" refers to "surface layer/pycnocline interface")

P_{net}^{sl*} represents the net accumulation of phytoplankton biomass in the surface layer normalized by the amount produced in the surface layer over one timestep This yuantity reflects the balance between production in the surtace layer and leakage out of the surface layer If $P_{net}^{sl*} = 1$, there are no leakage losses out of the surface layer, if $0 < P_{net}^{sl*} < 1$, there is positive net accumulation in the surface layer. despite the occurrence of leakage; if $P_{net}^{sl*} < 0$, then leakage dominates production, and the surface layer experiences net locc.

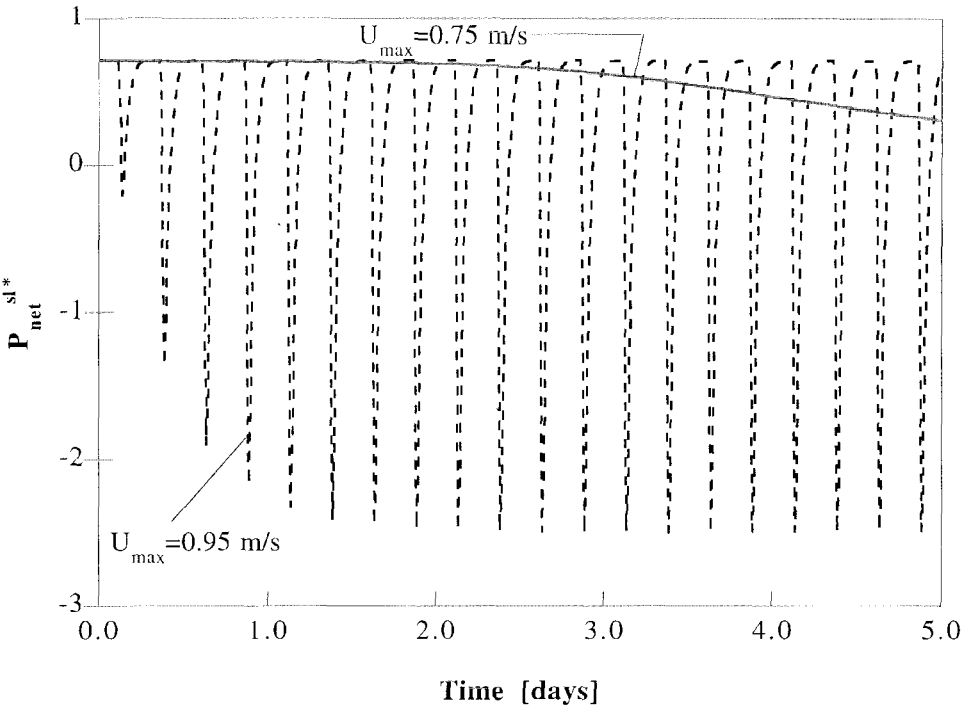

Figure 14. Evolution of P_{net}^{sl*} (net surface layer production) with time for two values of U_{max}: 0.75 and 0.95 m/s. In both cases, Z_m = 1 m, T_{pyc} = 1 m, ΔS = 5 psu, and W_s = 0.5 m/d.

Sustained positive values of P_{net}^{sl*} are associated with a bloom in the surface layer; whereas, sustained negative values of P_{net}^{sl*} are associated with a decline in surface layer biomass.

We have plotted P_{net}^{sl*} versus time for two cases which vary only by maximum tidal current speed (Fig. 14). BGO-SPEC was used to calculate turbulent diffusivities for both cases, with H = 15 m, Z_m = 1 m, T_{pyc} = 1 m, and ΔS = 5 psu. In V1D, W_s = 0.5 m/d and k_t = 1 m^{-1} for both cases. For reference, the lower U_{max} case (represented by the solid line) resulted in $\overline{B_5}$ = 29.3 mg chl a/m^3 (a large bloom); whereas, the higher U_{max} case (represented by the dashed line) yielded $\overline{B_5}$ = 6.6 mg chl a/m^3 (a much smaller bloom). The plot shows that P_{net}^{sl*} is always less than 1 for both cases, indicating that leakage fluxes are constantly occurring. For U_{max} = 0.95 m/s, a strong quarterdiurnal signal is evident, with P_{net}^{sl*} oscillating between positive and negative values. This indicates that the leakage contains a strong tidal mixing component which dominates the production during those portions of the semidiurnal tidal cycle when mixing is most intense. In between such leakage-dominated episodes, P_{net}^{sl*} returns to positive values, indicating that tidal mixing is weak enough such that production is temporarily able to exceed leakage. This result underscores the importance of semidiurnal tidal variability, as hypothesized by Koseff *et al.* (1993). For U_{max} = 0.75 m/s, only a faint tidal signal is evident, indicating that sinking is the most dominant of the two leakage processes for this case. Furthermore, for this low

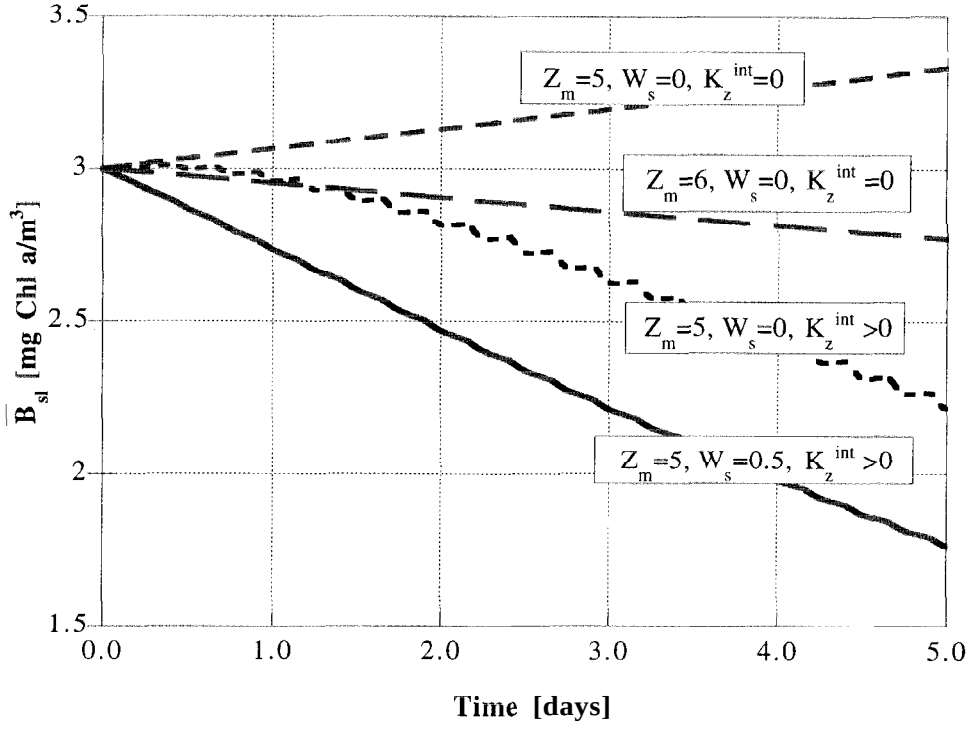

Figure 15. Surface layer averaged phytoplankton biomass versus time for four cases predicted by the phytoplankton model. For all cases, $k_t = 4\ m^{-1}$, which corresponds to a $Z_{cr} = 5.5$ m. "$K_z^{int} > 0$" means that the turbulent diffusivities used were those predicted by BGO; whereas. "$K_z^{int} = 0$" means that the turbulent diffusivities at the bottom of the surface layer were set to zero. For all cases, $T_{pyc} = 1$ m, U_{max} = 0.75 m/s, AS = 5 psu, and $a = 0.0$. Z_m and W_s are in [m] and [m/d], respectively.

U_{max} case, P_{net}^{sl*} is always positive, indicating that the surface layer biomass must be increasing in time, resulting in a much higher $\bar{B}_5$ than for the higher U_{max} case. The comparison of these two U_{max} cases may explain why blooms in SSFB always occur during periods of low tidal energy (Cloern, 1991; Cloern, 1996).

Earlier, we asserted that leakage from the surface layer is the reason for which our bloom predictions do not adhere to the traditional Sverdrup Critical Depth Model. We then explained the leakage mechanisms and demonstrated their effect on phytoplankton blooms. We now finally show that if all leakage is completely removed, our results are consistent with the SCDM. We have plotted $\bar{B}^{sl}$, the phytoplankton biomass averaged over the surface layer, versus time for four different cases (Fig. 15). Common to all cases are the following: H = 15 m, U_{max} = 0.75 m/s, T_{pyc} = 1 m, AS = 5 psu, and $k_t = 4\ m^{-1}$. For this light attenuation coefficient, Z_{cr} = 5.5 m. According to the critical depth model, Z_m = 5 m ($<Z_{cr}$) should result in a surface layer bloom for these irradiance conditions: whereas, Z_m = 6 m ($>Z_{cr}$) should not. We see that for Z_m = 5 m. the model predicts no bloom if

leakage of any sort occurs; whereas, if sinking and interfacial mixing are turned off, there is a surface layer bloom, as predicted by the SCDM. If $Z_m = 6$ m and all leakage is removed, there is no bloom, demonstrating further consistency with the SCDM under these ideal conditions.

5. Conclusions

In tidal estuaries, stratification and vertical mixing are highly dynamic processes, varying on timescales of hours to weeks. In systems with relatively strong tidal effects and weak freshwater influence, stratification may be only periodic on the semidiurnal timescale. We have shown that such periodic stratification (SIPS) does not increase the likelihood of a phytoplankton bloom over that of a constantly unstratified water column. Thus, with regard to its effects on phytoplankton blooms, SIPS is a physical regime closer to complete mixing than to persistent stratification, which greatly increases the likelihood of a bloom.

Although the persistence of stratification is important, the details of the persistent stratification are important as well. Specifically, surface-layer depth, thickness of the pycnocline, vertical density difference, and tidal current speed all weigh heavily in producing conditions which promote the onset of phytoplankton blooms. Our investigation of the effects of such hydrodynamic details leads to an explanation of why we might expect a range of functional relationships between phytoplankton growth and surface layer depth. First, there may be a non-monotonic relationship between phytoplankton population growth and surface layer depth. Thus, a shallower surface layer is not necessarily "better," from the perspective of maximizing phytoplankton production. This non-monotonic behavior is the result of the influence of Z_m, the surface layer depth, on several "competing" processes: (1) the interaction between turbulent mixing and sinking in the surface layer (i.e. Peclet number effects); (2) maximization of the average net growth rate in the surface layer; (3) minimization of turbulent leakage from the surface layer; and (4) minimization of the production occurring below the surface layer.

Second, we have shown that the traditional SCDM does not capture all the important processes governing phytoplankton bloom initiation in energetic shallow systems or in systems where surface layer mixing is not strong enough to counteract the sinking loss of phytoplankton (i.e. systems with high surface layer turbulent Peclet numbers). To apply to such systems, the SCDM would need to account for leakage of phytoplankton out of the surface layer, which can be responsible for the loss of a significant percentage of biomass produced in the surface layer. We have further shown that if all advective and turbulent diffusive leakage processes from the surface layer are eliminated, then model results comply exactly with the SCDM. Because of the large number of physical and biological parameters potentially controlling phytoplankton population growth in this type of system, it would be extremely difficult to collapse all those processes into one simple dimensionless expression, such as the SCDM.

What are the differences between shallow tidally driven systems and deeper pelagic

systems for which the traditional SCDM appears applicable? First, the primary source of turbulence in the ocean is the wind: whereas. for the system we have studied, turbulence is generated primarily at the bottom of the water column due to the interaction of the tidal current with the bottom roughness. In the ocean. therefore. as the wind blows, the surface layer is deepened and the euphotic zone may remain within the surface mixed layer. On the other hand. in shallow tidally dricen systems. the "real" mixed layer is the bottom layer. which, as turbulence continues to be generated, expands upward possibly into the euphotic zone, entraining phytoplankton cells and mixing them downward into aphotrc conditions. Where enhanced mixing may deepen the surface layer in the ocean. somewhat decreasing the average surface layer net growth rates. enhanced tidally driven mixing in the shallower system may have stronger negative effects on phytoplankton population growth by shallowing the surface layer and removing phytoplankton biomass from the euphotic zone.

A second difference is that the deeper wind-mixed surface layer may not incur as severe sinking losses as the shallower system, because greater turbulent diffusion in the deeper surface layer (due to both the wind source and the larger turbulent lengthscale) results in smaller turbulent Pcclet numbers in the surface layer Ihus. a deep wind-driven system may not have as much advective leakage as the shallower wind-free system For this reason. a deeper system may not have as strong of a non-monotonic relationship between phytoplankton growth and surface layer depth as the shallower tidally driven system has Inclusion of wind effects on the shallow system would most likely diminish advective surface layer losses and cause the relationship between phytoplankton concentration and surface layer depth to be more monotonic However. it is important to note that wind-induced mixing would likely enhance turbulent leakage of phytoplankton from the surface layer and augment the deviation from the SCDM. Similarly, we might expect that deeper systems could also experience enough turbulent surface layer leakage to deviate substantially from the SCDM.

In summary, the surface and bottom layers of a persistently stratified water column are not truly "decoupled" as has often been believed. This was pointed out by Sharples and Tett (1994) who, in order to match model results with observations of a mid-water chlorophyll maximum, had to allow some small degree of transport between the two layers. Thus, it may be best to conceptualize a pycnocline as a physical feature that merely detains phytoplankton cells in the surface layer (slowing their downward transport) as opposed to retaining them in the surface layer (completely preventing their downward transport). This vertical transport can occur by sinking or turbulent diffusion and, even at low levels. can severely reduce the likelihood of a bloom and lead to substantial departure from the traditional Sverdrup Critical Depth Model.

Acknowledgments LVL JKK and SGM wish to acknowledge the support of the NSF Division of Biological Oceanography through grant number OCE-9504081, as well as the Josephine de Karman Foundation. NASA, and EPA We thank Dr Alan Blumberg, who kindly tndde the BGO code available to us San Francisco Bay held data were provided by Dace Schoellhamer and Larry

Schemel, with support from the USGS Toxic Substance? Hydrology Program. The code for tidal current prediction was provided by Jeff Gartner. The authors thank the three anonymous reviewers for their helpful suggestions.

APPENDIX

Details of the phytoplankton model

a. The biological model

The model for phytoplankton growth is based on the following function for productivity by Jassby and Platt (1976):

$$P(z, t) = P_{max}[\tanh [aI(z, t)] - r] \tag{13}$$

where $P(z, t)$ is the biomass-specific rate of photosynthesis at depth z; P_{max} is the maximum (light-saturated) rate of photosynthesis: a defines the photosynthetic efficiency at low irradiance; $I(z, t)$ is the irradiance at depth z; and r is the respiration rate. expressed as a percentage of P_{max}. The net biomass-specific population growth rate is calculated using Eq. 13 to calculaie productivity and assuming that θ, the ratio of phytoplankton cellular carbon to chlorophyll *a*, is a constant equal to 50 (Cloern, 1991). Furthermore, we assume that ZP, losses to zooplankton grazing, are constant in depth and time. Thus, the relationship for the net phytoplankton growth rate is as follows:

$$\mu_{net}(z, t) = \frac{P(z, t)}{\theta} - ZP \tag{14}$$

The vertical distribution of photosynthetically active radiation is calculated from:

$$I(z_1, t) = I(0) \exp\left\{-[k_t + k_b(z_1, t)] \frac{\Delta z}{2}\right\} \tag{15}$$

$$I(z_j, t) = I(z_{j-1}, t) \exp\{-[k_t + k_b(z_j, t)\Delta z]\} \tag{16}$$

where $I(z_j)$ is the irradiance at the center of cell "j"; $I(0)$ is the mean daily surface irradiance; k_t is the mean light attenuation coefficient from abiotic sources of light absorption and scattering; and k_b is the component of light attenuation from phytoplankton biomass. Eq. 15 calculates irradiance for the top control volume, while Eq. 16 calculates irradiance for all other cells. k_t is usually taken to be constant in depth and time, while k_b is calculated for each point in the vertical. using Bannister's (1974) empirical constant of 0.016 [m^2/mg chl *a*] multiplied by the average biomass in the depth increment above that point. Irradiance is thus calculated incrementally with depth and varies with time. Relations (15) and (16) are for a uniformly spaced grid and are easily adapted for a nonuniform grid. See Table 1 for units and typical values of the parameters.

b. The finite volume discretization

We have discretized the phytoplankton transport equation (10) using a finite volume approach (MacCormack and Paullay, 1972) and associated staggered grid, which is divided into control volumes, or cells (Fig. 5). On this grid, B and μ_{net} (mass and sources/sinks) are defined at cell centers, while K_z and W, (all flux-related quantities) are defined at cell faces. Domain boundaries coincide with cell faces. Although benthic grazing is an overall sink for the water column, it is formulated as an advective flux; thus, it is defined at the bottom face of the bottom cell. The finite volume approach allows us to ensure that sources, sinks, fluxes, and accumulation exactly balance, preventing spurious numerical sources or sinks of mass.

A finite volume discretization originates with the "conservation law form" of the continuous equation. The defining characteristic of an equation cast in conservation law form is that the flux terms are combined into one term, which is the divergence of the total flux. The general phytoplankton transport equation in conservation law form is:

$$\frac{\partial B}{\partial t} + \nabla \cdot \mathbf{F} = Q \tag{17}$$

where:

$\mathbf{F}$ = total flux veclor $- \mathbf{F}_x + \mathbf{F}_y + \mathbf{F}_z$

$\mathbf{F}_k$ = total flux vector in k–direction $= \left(U_k B \quad K_k \frac{\partial B}{\partial k} \right) \mathbf{i}_k$

U_k = velocity in k–direction

$\mathbf{i}_k$ = unit vector in k–direction

Q = source term

Quantities in boldface are vector quantities. Integrating Eq. 17 over an arbitrary but constant control volume, V, and applying Gauss' Divergence Theorem, we get:

$$\frac{\partial \overline{B}}{\partial t} + \frac{1}{\mathbf{V}} \int_S \mathbf{F} \cdot \mathbf{dS} = \overline{Q} \tag{18}$$

where the overbar denotes an average over the control volume, V. S is the surface enclosing V, and **dS** is a surface element of S with the direction of the outward normal to S. Discretizing Eq. 18 for our 1D case ($\partial \mathbf{F}_x / \partial x = \partial \mathbf{F}_y / \partial y = 0$), we get the following:

$$\frac{\overline{B}_j^{n+1} - \overline{B}_j^n}{\Delta t} + \frac{1}{\mathbf{V}_j} \left[F_{z_{j-1/2}} S_{j+1/2} - F_{z_{j-1/2}} S_{j-1/2} \right] = \overline{Q}_j. \tag{19}$$

Subscripts refer to spatial location, whereas superscripts refer to the timestep. Fluxes and

surfaces in Eq. 19 are not in boldface because they are scalar quantities. Note that no time level has been assigned to the flux terms yet. Substituting the actual advective and diffusive fluxes in for F_z and the growth term in for $\overline{Q}$, realizing that for our 1D water column $S = 1$ and $V = \Delta z$, and making use of the fact that the benthic grazing term is zero everywhere but at the bottom boundary, Eq. 19 becomes the following for all interior cells:

$$B_j^{n+1} = B_j^n - \frac{\Delta t}{\Delta z}[(W_s B^*)_{j+1/2}^n - (W_s B^*)_{j-1/2}^n] + \frac{\Delta t}{\Delta z}\left[\left(K_z \frac{\partial B}{\partial z}\right)_{j+1/2}^{n+1} - \left(K_z \frac{\partial B}{\partial z}\right)_{j-1/2}^{n+1}\right] + \Delta t(\mu_{net_j} B_j)^{n+1}. \quad (20)$$

Note here that the overbars have been dropped, since we are taking the concentration at the center of a cell to represent the average over the cell. B^*, which appears in the advection terms, represents an estimate of B at the cell face, since this approach does not naturally locate B at faces. The above semi-discretization is for an explicit treatment of advective terms and an implicit treatment of diffusion and growth. Actually, our code allows for any degree of implicitness for the diffusion and growth terms; however, we typically opt to solve those terms implicitly.

The turbulent diffusivities (K_z's) are obtained from the BGO code, and are located exactly where they are needed—at the cell faces. Furthermore, the staggered grid conveniently locates biomass concentrations between faces such that centered differences are easily implemented for the spatial derivatives in the diffusion terms. The implicit treatment of diffusion produces a tridiagonal system of equations, which is solved using the Thomas Algorithm.

The advection terms are slightly more challenging. In order to calculate B^*, our estimate of B at the cell face, we use Leonard's (1979) QUICK (Quadratic Upstream Interpolation for Convective Kinematics) method. QUICK uses a three-point upstream-weighted quadratic interpolation for the concentration at a cell face. This method helps to minimize instabilities associated with central differencing of convection-dominated problems, and it does not produce the significant artificial diffusion introduced by classical upwind methods. The QUICK estimate of B* is of the following form:

$$B_{j+1/2}^* = \frac{(B_{j+1}^n + B_j^n)}{2} - \frac{(B_{j+1}^n - 2B_j^n + B_{j-1}^n)}{8} \quad (21)$$

c. Boundary conditions

At the top of the water column, we want to enforce zero advective flux and zero diffusive flux of phytoplankton through the surface. To effect this condition, the advective and diffusive flux terms at face $j = 1/2$ (the top face of the top control volume) essentially disappear from the discretization (Eq. 20), since those terms are zero. Thus, Eq. 20 applied

to the top control volume (cell $j = 1$) becomes the following:

$$B_1^{n+1} = B_1^n - \frac{\Delta t}{\Delta z}[(W_s B^*)_{3/2}^n] + \frac{\Delta t}{\Delta z}\left[\left(K_z \frac{\partial B}{\partial z}\right)_{3/2}^{n+1}\right] + \Delta t(\mu_{\text{net}_1} B_1)^{n+1}. \tag{22}$$

At the bottom of the water column, we want to allow for a possible flux due to benthic grazing but enforce zero flux for diffusion and sinking. This configuration allows for accumulation in the bottom cell, for example, if sinking dominates mixing and grazing. To enforce these conditions, the benthic grazing reappears in the flux term for face $j = nmax + 1/2$ (see Fig. 5), and, similar to the treatment of the top surface, the sinking and mixing term fall out, since they are zero. Although the benthic grazing term is essentially an advective flux, we do not implement QUICK to estimate B at the bottom face, since doing so would require a "phantom" point outside of the actual flow domain. We therefore use a simple upwind treatment for that particular case. Applying all these conditions, Eq. 20 becomes the following for the bottom control volume (cell $j = nmax$):

$$\begin{aligned} B_{nmax}^{n+1} = B_{nmax}^n - \frac{\Delta t}{\Delta z}[-(W_s B^*)_{nmax-1/2}^n] + \frac{\Delta t}{\Delta z}\left[-\left(K_z \frac{\partial B}{\partial z}\right)_{nmax-1/2}^{n+1}\right] \\ + \Delta t(\mu_{net_{nmax}} B_{nmax})^{n+1} - \frac{\Delta t}{\Delta z}(\alpha B_{nmax}^{n+1}). \end{aligned} \tag{23}$$

Note that Eq. 23 shows the grazing term to be treated implicitly in time. Actually, our code allows that term, like the diffusion and growth terms, to be treated with any degree of implicitness; however, we usually opt for fully implicit treatment.

d. Accuracy and stability

The application of QUICK to the sinking terms and central differencing to the diffusion terms leads to second order spatial accuracy, and minimal artificial diffusion is incurred by our treatment of the advection. Time accuracy is first order. A Von Neumann stability analysis (Hirsch, 1988) performed on the advection-diffusion equation (with explicit treatment of the advection and implicit treatment of the diffusion) yields the following stability criterion:

$$\frac{1 - \frac{c}{2} + \frac{13}{8}c^2}{(1 + 2s)^2} \leq 1 \tag{24}$$

where:

$$c = \frac{W_s \Delta t}{\Delta z} \text{ and } s = \frac{K_z \Delta t}{\Delta z^2}.$$

Thus, as diffusivities get smaller, the more prone the scheme is to produce oscillations; however, use of QUICK on the advection terms makes the solution much more resistant to oscillations than if linear interpolation, for instance, were used. In order to ensure that diffusivities never reach a value low enough (e.g. in strongly stratified cases) to induce oscillations, the VID phytoplankton code imposes a minimum K_z value on all diffusivities. An additional stability criterion which relates to grazing at the bottom boundary is the following Courant condition:

$$\frac{\alpha \Delta t}{\Delta z} \leq 1. \tag{25}$$

REFERENCES

Abraham. G. 1988. Turbulence and mixing in stratified tidal flow, in Physical Processes in Estuaries, J. Dronkers and W. van Leussen, ed., New York, Springer-Verlag. 149–180.

Armi, L. and D. M. Farmer. 1986. Maximal two-layer exchange through a contraction with barotropic net flow. J. Fluid Mech., 164, 27–51.

Bannister, T. T. 1974. A general theory of steady state phytoplankton growth in a nutrient saturated mixed layer. Limnol. Oceanogr., 19, 13–30.

Blumberg, A. F.. B. Galperin and D. J. O'Connor. 1992. Modeling vertical structure of open-channel flows. J. Hydr. Eng.. *118*, 1119–1134.

Blumberg, A. F. and D. M. Goodrich. 1990. Modeling of wind-induced stratification in Chesapeake Bay. Estuaries, *13*, 236–249.

Blumberg. A. F. and G. L. Mellor. 1987. A description of a three-dimensional coastal ocean circulation model. *in* Three Dimensional Coastal Ocean Models, N. S. Heaps, ed.. American Geophysical Union, Washington D.C.. 1–16.

Cheng. R. T. and J. W. Gartner. 1985. Harmonic analysis of tides and tidal currents in South San Francisco Bay, California. Estuar. Coast. Shelf Sci., *21*, 57–74.

Cloern, J. E. 1982. Does the benthos control phytoplankton biomass in South San Francisco Bay? Mar. Ecol. Prog. Ser.. *9*, 191-202.

———— 1987. Turbidity as a control on phytoplankton biomass and productivity in estuaries. Cont. Shelf Res., *7*, 1367-1381.

———— 1991. Tidal stirring and phytoplankton bloom dynamics in an estuary. J. Mar. Res., 49. 203–221.

———— 1996. Phytoplankton bloom dynamics in coastal ecosystems: a review with some general lessons from sustained investigation of San Francisco Bay, California. Rev. Geophyr.. 34, 127–168.

Edmunds. J. L., B. E. Cole, J. E. Cloern. and R. G. Dufford. 1997. Studies of the San Francisco Bay. California, Estuarine Ecosystem: Pilot Regional Monitoring Results, 1995. U. S. Geol. Survey Open-File Report, 97–15.

Franks. P. J. S. and C. Chen. 1996. Plankton production in tidal fronts: a model of Georges Bank in summer. J. Mar. Res., *54*, 631–651.

Friebel. M. F., L. F. Trujillo, and K. L. Markham. 1996. Water resources data for California, Water Year 1995, Volume 2, Pacific slope basins from Arroyo Grande to Oregon state line except Central Valley. U.S. Geological Survey Water-Data Report, CA-95-2. 360 pp.

Galperin, B., L. H. Kantha. S. Hassid and A. Rosati. 1988. A quasi-equilibrium turbulent energy model for geophysical flows. J. Atmos. Sci., *45*, 55–62.

Gran, H. H. and T. Braarud. 1935. A quantitative study on the phytoplankton of the Bay of Fundy and the Gulf of Maine including observations on hydrography. chemistry and niorbidity. J. Biol. Bd. Can., *1,* 219–467.

Gregg, M. C. 1987. Diapycnal mixing in the thermocline: a review. J. Geophys. Res. (Oceans), *92,* 5249–5286.

Haas, L. W., S. J. Hastings and K. L. Webb. 1981. Phytoplankton responses to a stratification-mixing cycle in the York River estuary during late summer, *in* Estuaries and Nutrients. B. J. Neilson and L. E. Cronin, eds., Humana, Clifton, New Jersey, 619–636.

Hamblin, P. F. 1989. Observations and model of sediment transport near the turbidity maximum of the Upper Saint Lawrence Estuary. J. Geophys. Res. (Oceans), 94, 14419–14428.

Hansen, D. V. and M. Rattray. 1965. Gravitational circulation in straits and estuaries. J. Mar. Res., 23, 104–122.

Herman, P. M. J. 1993. A set of models to investigate the role of benthic suspension feeders in estuarine ecosystems, *in* NATO ASI Series, Vol. G33: Bivalve Filter Feeders in Estuarine and Coastal Ecosystem Processes, R. F. Dame, ed., Springer-Verlag, 421–454.

Hirsch, C. 1988. Numerical Computation of Internal and External Flows, Vol. 1: Fundamentals of Numerical Discretization, Wiley-Interscience, 515 pp.

Jassby, A. D., W. J. Kimmerer, S. G. Monismith. C. Armor, J. E. Cloern, T. M. Powell, J. R. Schubel, and T. J. Vendlinski. 1995. Isohaline position as a habitat indicator for estuarine populations. Ecol. Appl., 5, 272–289.

Jassby. A. D. and T. Platt. 1976. Mathematical formulation of the relationship between photosynthesis and light for phytoplankton. Limnol. Oceanogr., *21,* 540–547.

Jay, D. A. and J. D. Musiak. 1996. Internal tidal symmetry in chanel flows "origins and consequences," *in* Mixing Processes in Estuaries and Coastal Seas, C. Pattiaratchi, ed., Amer. Geophys. Union, 211–249.

Jay, D. A. and J. D. Smith. 1990a. Residual circulation in shallow estuaries, 2. Weakly straiified and partially mixed estuaries. J. Geophys. Res., *95,* 733–748.

——— 1990b. Circulation, density distribution and neap-spring transitions in the Columbia River Estuary. Prog. Oceanogr., *25,* 81–112.

Koseff, J. R., J. K. Holen, S. G. Monismith and J. E. Cloern. 1993. Coupled effects of vertical mixing and benthic grazing on phytoplankton populations in shallow, turbid estuaries. J. Mar. Res., *51,* 843–868.

Leonard. B. P. 1979. A stable and accurate convective modelling procedure based on quadratic upstream interpolation. Comp. Methods Appl. Mech. Eng., 19, 59–98.

MacCormack, R. W. and A. J. Paullay. 1972. Computational efficiency achieved by time splitting of finite difference operators. AIAA Paper, San Diego, 72–154.

Martin, J. H., R. M. Gordon and S. E. Fitzwater. 1991. The case for iron. Limnol. Oceanogr., 36, 1793–1802.

Mellor, G. L. and T. Yamada. 1982. Development of a turbulence closure model for geophysical fluid problems. Rev. Geophys. Space Phys., *20,* 851–875.

Monismith, S. G. and D. A. Fong. 1996. A simple model of mixing in stratified tidal flows. J. Geophys. Res., *101,* 28583–28597.

Monismith, S. G., J. R. Burau and M. T. Stacey. 1996. Stratification dynamics and gravitational circulation in Northern San Francisco Bay, *in* San Francisco Bay: The Ecosystem, J. T. Hollibaugh, ed., AAAS, San Francisco, 123–153.

Nepf, H. M. and W. R. Geyer. 1996. Intratidal variations in stratification and mixing in the Hudson estuary. J. Geophys. Res. (Oceans), *101,* 12079–12086.

Nunes Vaz, R. A., G. W. Lennon and J. R. de Silva Samarasinghe. 1989. The negative role of turbulence in estuarine mass transport. Estur. Coast. Shelf Sci.. 28. 361–377.

Nunes Vaz, R. A. and J. H. Simpson. 1994. Turbulence closure modeling of estuarine stratification. J. Geophys. Res., *99,* No. C8. 16,133–16,160.

Obata, A., J. Ishizaka and M. Endoh. 1996. Global verification of critical depth theory for phytoplankton bloom with climatological *in situ* temperature and satellite ocean color data. J. Geophys. Res,, 101, 20,657–20,667.

O'Donnell, J. 1993. Surface fronts in estuaries: a review. Estuaries. 16, 12–39.

Officer. C. B. 1976. Physical Oceanography of Estuaries (and associated coastal waters). Wiley, New York. 446 pp.

Platt, T., D. F. Bird and S. Sathyendranath. 1991. Critical depth and marine primary production. Proc. Roy. Soc. London, Series B, Biol. Ser.. 246, 205–218.

Riley, G. E. 1942. The relationship of vertical turbulence and spring diatom flowerings. J. Mar. Res., 5, 54–71.

Sharples. J.. J. H. Simpson and J. M. Brubaker. 1994. Observations and modelling of periodic stratilication in the upper York River Estuary, Virginia. Estuar. Coast. Shelf Sci., *38,* 301–312.

Sharples. J. and P. Tett. 1994. Modelling the effect of physical variability on the midwater chlorophyll maximum. J. Mar. Res.. 52, 219–238.

Simpson, J. H., J. Brown, J. Matthews and G. Allen. 1990. Tidal straining. density currents, and stirring in the control of estuarine stratification. Estuaries. *13,* 125–132.

Simpson, J. H. and J. Sharples. 1991. Dynamically-active models in the prediction of estuarine stratification, *in* Dynamics and Exchanges in Estuaries and the Coastal Zone, D. Prandle, ed., Springer-Verlag. New York, 101–113.

Simpson, J. H., J. Sharples and T. P. Rippeth. 1991. A prescriptive model of stratification induced by freshwater runoff. Estuar. Coast. Shelf Sci., 33, 23–35.

Sinclair. M. 1978. Summer phytoplankton variability in the lower St. Lawrence estuary. J. Fish. Res. Bd. Can.. 35, 1171–1185.

Sinclair, M., D. V. Subba Rao and R. Couture. 1981. Phytoplankton temporal distribution in estuaries. Oceanol. Acta, *4,* 239–246.

Snietacek, V. and U. Passow. 1990. Spring bloom initiation and Sverdrup's critical-depth model. Limnol. Oceanogr., *35,* 228–234.

Sverdrup. *H.* U. 1953. On conditions for the vernal blooming of phytoplankton. J. Conseil Exp. Mer.. *18,* 287–295.

Taylor, A. H. and J. A. Stephens. 1993. Diurnal variations of convective mixing and the spring bloom of phytoplankton. Deep-Sea Res. II, *40,* 389–408.

Uncles, R. J. and J. A. Stephens. 1990. The structure of vertical current profiles in a macrotidal, partly-mixed estuary. Estuaries, 13, 349–361.

Winter, D. F.. K. Banse and G. C. Anderson. 1975. The dynamics of phytoplankton blooms in Puget Sound, a fjord in the northwestern United States. Mar. Biol., 29, 139–176.

Received: *25 February 1997;* revised: *19 January, 1998.*